Granulocytic cells of adult mouse BM express CD11b and high amounts of Gr-1. The absolute number of $CD11b^+/Gr\text{-}1^+$ granulocytes was lower in MT1-$MMP^{-/-}$ than in MT1-$MMP^{+/+}$ BM cells (Figure 3D). G-CSF is a growth, differentiation, and activating factor for neutrophils and their precursors. Regardless of the observed neutropenia, no difference in *G-CSF* (Figure 3E) or thrombopoietin (*Tpo*; data not shown) expression was observed in the BM cells of these mice, indicating that other factors might be responsible for the impaired myelopoiesis.

MT1-MMP deficiency reduces stromal cell–derived cytokine production

Chimera experiments indicated that the observed hematopoietic defect in MT1-MMP–deficient mice was in part because of a niche defect, suggesting that dysregulated production of stromal cell–derived cytokine(s) may be responsible for the hematopoietic differentiation block observed in MT1-$MMP^{-/-}$ mice. BM and thymic stromal cells produce IL-7.[36] Plasma levels of the stromal cell–derived factors KitL, SDF-1α, and IL-7 were lower in MT1-$MMP^{-/-}$ mice than in MT1-$MMP^{+/+}$ mice (Figure 4A-C). We observed a reduced number of $nestin^+$ niche cells in MT1-$MMP^{-/-}$ mice and, interestingly, $nestin^+$ niche cells highly express KitL and SDF-1.[31] In accordance with these data, MT1-$MMP^{-/-}$ BM cells and MT1-$MMP^{-/-}$ primary stromal cells showed lower mRNA expression of *IL-7, KitL*, and *SDF-1α/CXCL12* compared with MT1-$MMP^{+/+}$ cells (Figure 4D, supplemental Figure 1). In addition, very few primary stromal cells grew in cultures established using MT1-$MMP^{-/-}$ BM cells (supplemental Figure 1).

To exclude the possibility that the growth/chemokine factor decrease in MT1-$MMP^{-/-}$ mice was because of a lower number of the growth factor–producing stromal cells, we modulated MT1-MMP expression on a murine stromal cell line (MS-5). Overexpression of MT1-MMP in MS-5 stromal cells (MT1-MMP TF) increased *KitL, SDF-1α*, and *IL-7* gene expression (Figure 4E). In contrast, MT1-MMP knock down in MS-5 murine stromal cells using shRNA (*MT1-MMP KD*) reduced the expression of *KitL, SDF-1α*, and *IL-7* mRNA than control MS-5 cells (Figure 4F). Consistent with this result, less KitL, SDF-1α, and IL-7 protein was detected in supernatants of MT1-MMP KD cultures compared with control cultures as determined by ELISA (Figure 4G). The frequency of CXCR4 (the SDF-1 receptor) and c-Kit (the KitL receptor) expressing $Sca\text{-}1^+$ MT1-$MMP^{-/-}$ BMMCs was not significantly changed (data not shown). These data indicate that loss of MT1-MMP activity in stromal cells reduced signaling by IL-7, KitL, and SDF-1α, factors known to regulate B and T lymphopoiesis and erythropoiesis.

We next examined the release and expression of these factors by primary *MEFs*. Confirming our BM cell and primary stromal cell cytokine/chemokine data, low expression of *KitL, SDF-1α*, and *IL-7* was found in MT1-$MMP^{-/-}$ MEFs (Figure 4H-I).

To investigate whether the observed impaired production of cytokines/chemokines would also result in impaired function, we set up an MEF feeder–based culture supplemented with IL-3. Whereas Lin^- cells differentiated in MT1-$MMP^{+/+}$ MEF-supported cultures, the number of $CD11b^+/Gr\text{-}1^+$ cells in MT1-$MMP^{-/-}$ cultures did not change significantly (Figure 4J). Addition of neutralizing Abs against KitL confirmed that the observed myeloid cell differentiation was mainly because of the KitL that was released by the cultures.

We set up a migration assay to investigate SDF-1α function. Lin^- cells derived from BM cells migrated toward an MT1-$MMP^{+/+}$ MEF supernatant, a process that is mediated by SDF-1, as shown by using neutralizing Abs against SDF-1. In contrast, no migration of Lin^- cells was observed toward an MT1-$MMP^{-/-}$ supernatant (Figure 4K).

MT1-MMP increases cytokine/chemokine production in niche cells by suppressing HIF-1α

The *HIF* gene is known to regulate VEGF, placental growth factor, angiopoietin 2, platelet-derived growth factor-B, SDF-1α, Epo, and KitL/SCF expression.[7] HIF-1α activity under normoxia depends on the FIH-1. FIH1-mediated hydroxylation disrupts a critical interaction between HIFα and the coactivators p300/CBP, impairing HIF transcriptional activity.[37,38] To determine whether HIF signaling is involved in MT1-MMP modulation of hematopoietic differentiation, we assessed HIF-1α, HIF-2α, and FIH-1 protein levels in MT1-MMP knockdown and control MS-5 cells. MT1-MMP knockdown did not affect HIF-1α or HIF-2α protein expression (supplemental Figure 2), but did up-regulate FIH-1 protein expression within the cytosol of MS-5 cells (Figure 5A), where FIH-1 can prevent HIF-1α binding to the transcriptional coactivator p300/CBP thereby blocking HIF-1-induced transcription of genes such as SDF-1 and KitL.[39] Immunohistochemical analysis showed that less $nestin^+$ stromal cells coexpressing FIH-1 were found in MT1-$MMP^{-/-}$ BM cells than in MT1-$MMP^{+/+}$ BM cells (Figure 5B). These findings are consistent with previous data that, in monocytes, the cytoplasmic tail of MT1-MMP binds to FIH-1, leading to inhibition of FIH-1 activity by its inhibitor, Mint3/APBA3.[23]

HIF-1 immunostaining showed that HIF-1, in contrast to its expression in MT1-$MMP^{+/+}$ BM cells, was preferentially expressed in the cytoplasm of MT1-$MMP^{-/-}$ BM cells (Figure 5C).

Our data suggested that MT1-MMP can activate the HIF1 pathway in stromal cells as it does in monocytes. We therefore hypothesized that FIH-1 overexpression in stromal cells would cause a reduction in cytokine/chemokine production, which was indeed the case (Figure 5D-F). These data suggested that FIH-1 overexpression reduced SDF-1, KitL, and IL-7 gene transcription in stromal cells. Furthermore, although the knockdown efficiency of FIH-1 by shRNA was only 30%, FIH-1 knockdown rescued *KitL, SDF-1α*, and *IL-7* gene expression in MT1-MMP knockdown (70% reduction by siRNA) MS-5 cells (Figure 5G-I) indicating that the decreased HIF-mediated cytokine gene transcription in MT1-MMP knockdown stromal cells can be partially rescued by blocking FIH-1 activity. These data highlight the importance of MT1-MMP–mediated HIF-1 activation for the transcriptional regulation of critical hematopoietic niche factors.

Exogenous SDF-1α and KitL addition restores leukopenia and thrombopenia in MT1-$MMP^{-/-}$ mice

Finally, we asked whether growth factor addition would rescue the observed block in leukopenia and thrombopenia because of MT1-MMP deficiency. Indeed, addition of recombinant IL-7 to MT1-$MMP^{-/-}$ or wild-type BMMC cultures induced a similar number of B-cell colonies (CFU–IL-7) in the MT1-$MMP^{-/-}$ as in the wild-type cells (Figure 6A).

MS-5 cells support myeloid cell differentiation of Lin^- wild-type cells in vitro. However, fewer GFP^+ hematopoietic cells were generated from Lin^- wild-type BM cells on MT1-MMP KD MS-5 stromal cells than on control MS-5 cells. Addition of KitL restored hematopoietic cell growth on the MT1-MMP KD MS-5 feeder cultures (Figure 6B).

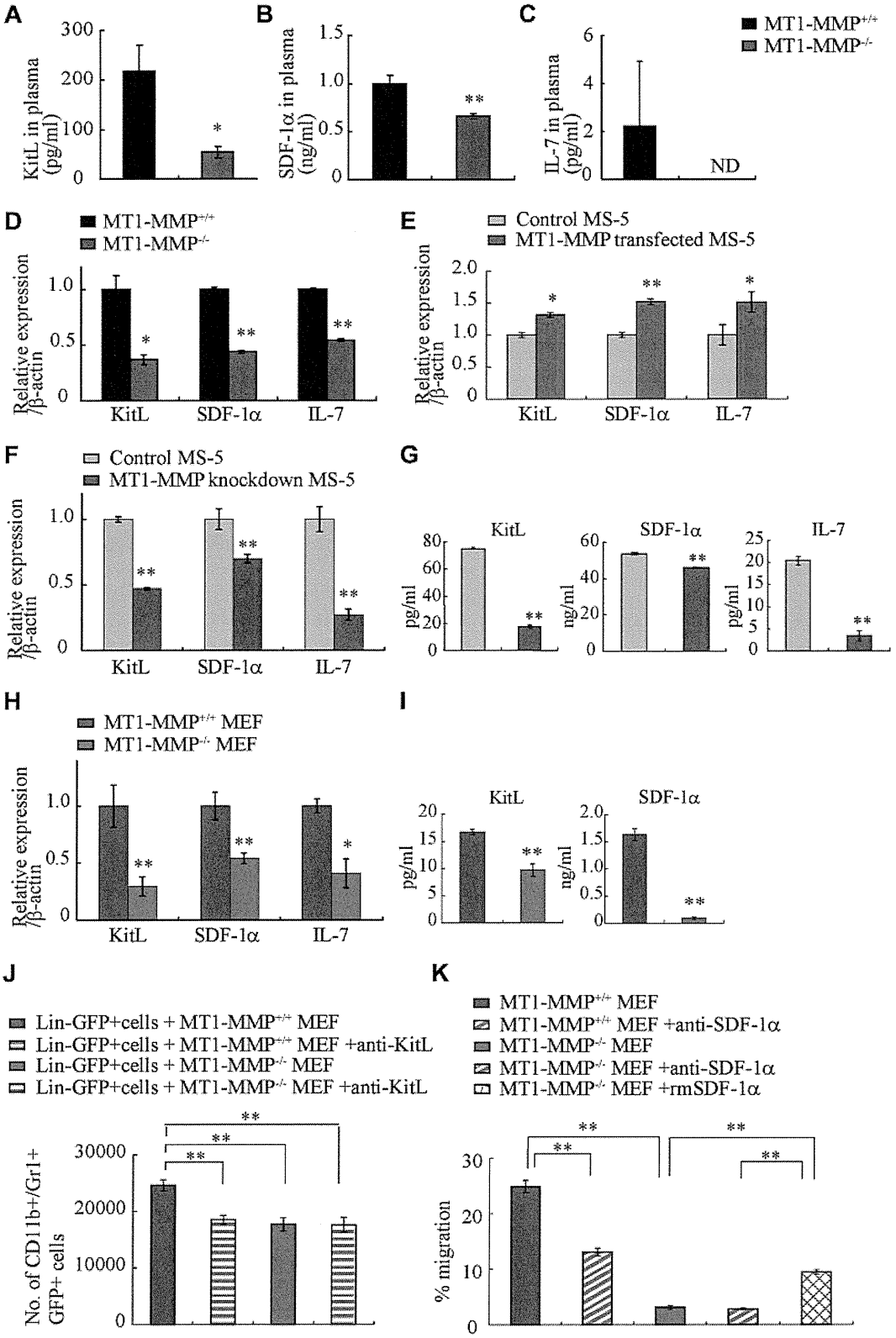

Figure 4. MT1-MMP deficiency prevents transcription of niche chemokines/cytokines. (A-C) KitL, SDF-1α, and IL-7 plasma levels in MT1-MMP$^{+/+}$ and MT1-MMP$^{-/-}$ plasma were measured by ELISA (n > 6). *KitL*, *SDF-1α*, and *IL-7* gene expression in (D) total BM cells, (E) MS-5 control and MT1-MMP–overexpressing cells, and (F) MT1-MMP knockdown (KD) and control MS-5 cells were analyzed using real-time PCR. The results are expressed relative to expression of a *β-actin*. (G) KitL, SDF-1α, and IL-7 protein levels in MT1-MMP knockdown (KD) and control MS-5 cell-culture supernatants were determined by ELISA. (H) *KitL*, *SDF-1α*, and *IL-7* gene expression in MT1-MMP$^{+/+}$ and MT1-MMP$^{-/-}$ MEF cells was determined using real-time PCR. The results are expressed relative to expression of *β-actin*. (I) KitL and SDF-1α protein levels in the indicated MEF cell-culture supernatants were evaluated by ELISA. (J) Lin^{-}GFP^{+} cells were cultured on MT1-MMP$^{+/+}$ and MT1-MMP$^{-/-}$ MEF cells in the presence or absence of neutralizing Abs against KitL. The number of CD11b^{+}Gr1^{+} cells was assessed after 7 days by FACS (n = 5). (K) Lin^{-} cells were plated in transwells. MT1-MMP$^{+/+}$ and MT1-MMP$^{-/-}$ MEF cell-culture supernatants supplemented with recombinant SDF-1α were added to the lower chamber. Neutralizing Abs against SDF-1α were added to both chambers. The percentage of migrated cells was determined (n = 9 from 2 independent experiments). Errors in bar graphs are SEM; $^{*}P < .05$, $^{**}P < .01$. Data shown are representative of 3 to 4 independent experiments.

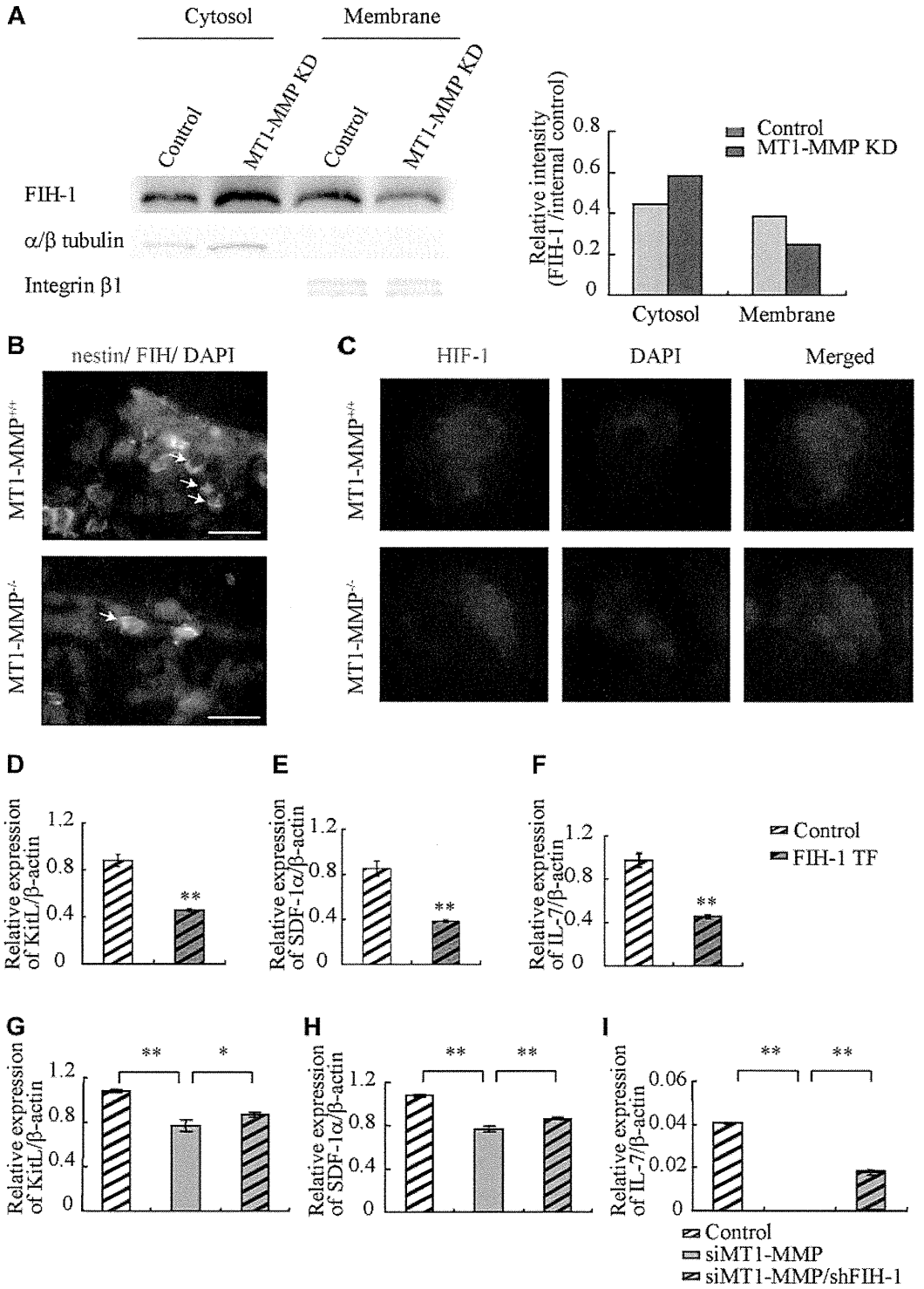

Figure 5. MT1-MMP deficiency prevents HIF-mediated transcription of niche factors. (A) FIH-1 expression in subcellular fractions was analyzed by Western blotting. α/β tubulin and integrin-β1 are representative cytosolic and membrane proteins, respectively. (B) Representative images of immunofluorescent staining of nestin (green fluorescence) and FIH-1 (red fluorescence) in BM sections derived from MT1-MMP$^{+/+}$ and MT1-MMP$^{-/-}$ mice. The arrows indicate nestin^{+}/FIH-1 cells. Nuclei were counterstained with DAPI (blue; bars, 100 μm). (C) Representative images of immunofluorescent staining of HIF-1α (green fluorescence) in BM cells derived from MT1-MMP$^{+/+}$ and MT1-MMP$^{-/-}$ mice. Nuclei were counterstained with DAPI (blue). (D-I) *KitL*, *SDF-1α* and *IL-7* gene expression in (D-F) MS-5 cells overexpressing FIH-1, and (G-I) in MT1-MMP–deficient MS-5 cells with or without *FIH-1* knockdown as analyzed using real-time PCR. The results are expressed relative to expression of a *β-actin*, which was set at 1.0. Data shown are representative of 3 to 4 independent experiments.

Similarly, KitL treatment restored WBC and PLT numbers in the PB in MT1-MMP$^{-/-}$ mice to the values of wild-type controls (Figure 6C-D) and a single injection of SDF-1α increased both WBC and PLT counts in the PB of MT1-MMP$^{-/-}$ mice 2 days after injection (Figure 6E-F). Although hematopoietic cell growth was restored in MT1-MMP$^{-/-}$ mice by injection of KitL or SDF-1, survival was not improved (data not shown).

Collectively, these results suggest that MT1-MMP alters the HSC niche by modulating HIF signaling, which promotes cytokine production and enhances cell differentiation and migration.

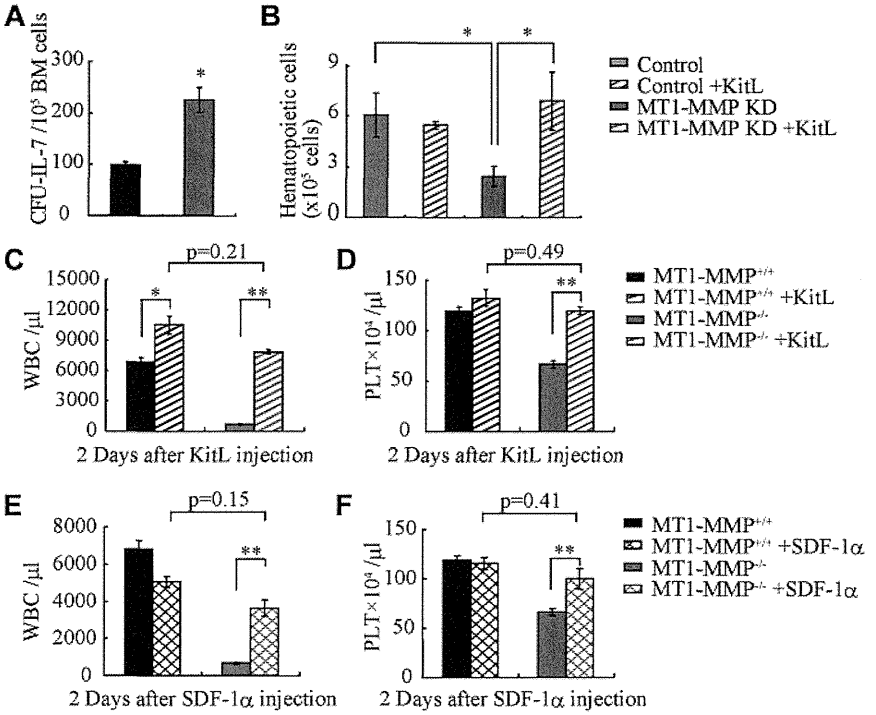

Figure 6. MT1-MMP–deficient mice have a defective BM stromal niche with impaired terminal differentiation because of impaired release of HIF-1α–associated factors. (A) Number of colonies in IL-7–containing cultures of MT1-MMP$^{+/+}$ and MT1-MMP$^{-/-}$ BM cells (n = 3). (B) Coculture of wild-type Lin$^-$ BM GFP$^+$ cells on confluent MT1-MMP knockdown or control MS-5 cells with/without KitL. (C-D) PB WBCs (C) and PLT (D) after KitL injections into MT1-MMP$^{+/+}$ (n ≥ 10) and MT1-MMP$^{-/-}$ mice (n = 3). (E-F) PB WBCs (E) and PLT (F) counts 2 days after initiation of SDF-1 treatment of MT1-MMP$^{+/+}$ (n ≥ 10) and MT1-MMP$^{-/-}$ mice (n = 2). Errors in bar graphs are SEM; $^*P < .05$, $^{**}P < .01$.

Discussion

In this report, we identified MT1-MMP as a key player of postnatal hematopoiesis. We demonstrate that MT1-MMP–expressing cells serve as key links between the HIF-1 regulatory system and transcriptional regulation of vital niche chemokines/cytokines necessary for HSC maintenance and cell differentiation (Figure 7). Specifically, we show that MT1-MMP deficiency leads to impairment of steady-state hematopoiesis because of a reduced HSC pool and a trilineage differentiation block. Mechanistically, we provide evidence that MT1-MMP deficiency in niche/stromal cells increases cytosolic FIH1 on expense of the membrane-associated FIH1 expression, thereby preventing transcription of the HIF-responsive genes EPO, KitL, IL-7, and SDF-1α. Thus, this study identifies MT1-MMP as a key molecular link between hypoxia and the regulation of vital HSC niche factors.

We reported that MMP-9 and plasminogen activation is important for the ectodomain shedding of the hematopoietic growth factor like KitL.[10,19] MT1-MMP can activate various proteases, including plasminogen or MMP-2, which in turn can activate MMP-9. It has been reported that MMP-2 activation can process

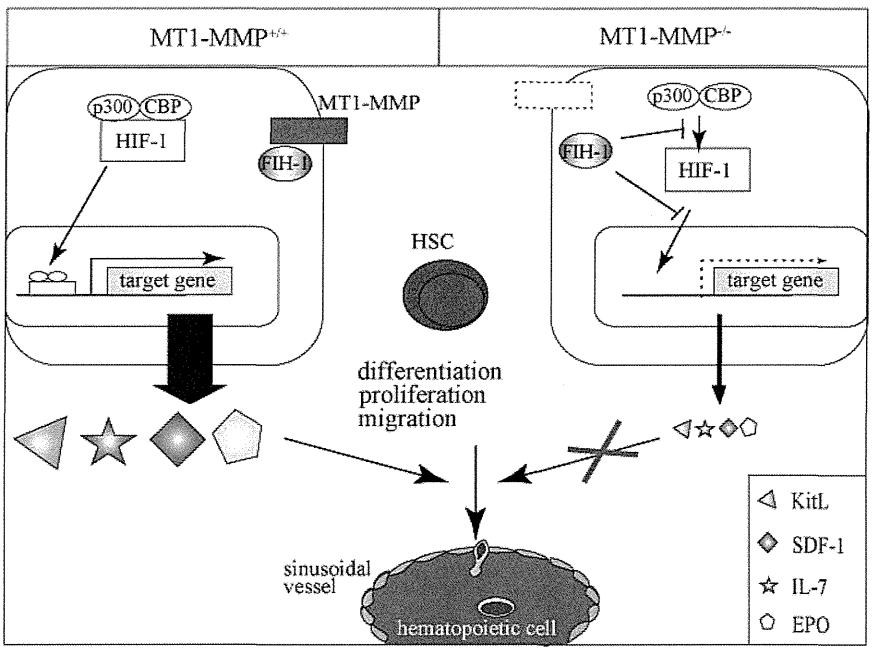

Figure 7. Proposed model of the role of MT1-MMP–expressing niche cells, which serve as key links between the HIF-1 regulatory system and transcriptional regulation of vital niche chemokines/cytokines necessary for HSC maintenance and cell differentiation. MT1-MMP deficiency in niche cells up-regulates FIH1 expression, thereby preventing transcription of the HIF-responsive genes *EPO*, *KitL*, *IL-7*, and *SDF-1α*. MT1-MMP deficiency leads to impaired steady-state hematopoiesis because of a trilineage differentiation block.

SDF-1/CXCL12.[40] We are currently examining whether ectodomain shedding by MT1-MMP–activated MMPs could be another reason for the low cytokine levels observed in MT1-MMP$^{-/-}$ mice.

Other known modulators of the BM and of niches such as the cancer stem cell niche, including vascular endothelial growth factor-A, angiopoietin 2, placental growth factor, and platelet-derived growth factor B, are also HIF-regulated target genes and therefore might also depend on MT1-MMP function.[7,8,41-43] But further studies will be needed to proof this concept.

Using BM chimeras generated using MT1-MMP$^{-/-}$ and MT1-MMP$^{+/+}$ donor cells, we showed that the developmental T-cell differentiation arrest observed in MT1-MMP$^{-/-}$ mice was mainly because of a niche defect, and not because of the impaired stem cell pool observed in these mice. In MT1-MMP$^{-/-}$ mice, we found preferential differentiation into CD4 SP thymocytes, which is most likely because of impaired Notch signaling.[44] Indeed, a recent study demonstrated that MT1-MMP directly cleaves Dll-1, a Notch ligand on BM stromal cells.[45] The continued presence of Dll-1 is required for T-cell commitment and maintenance at the DN1 and DN2 stages of thymocyte development. In the absence of Notch signaling, the developing DN1 and DN2 thymocytes adopt a NK-cell fate by default, a phenomena that we indeed observed in the MT1-MMP$^{-/-}$ mice.[46]

IL-7 signaling and Notch signaling are implicated in B-cell lymphopoiesis.[47] We found that HSC differentiation toward B lymphocytes was compromised in MT1-MMP–deficient BM cells. The long-term proliferation capacity of BM pre-B1 cells is known to be critically dependent on KitL and IL-7 expression and signaling, factors that we have shown require the presence of MT1-MMP for their expression.[48,49] Furthermore, we provide evidence that MT1-MMP deficiency in stromal cells also impairs the expression of SDF-1α, which is a key regulator of B-cell lymphopoiesis and BM myelopoiesis.[50] Our data are consistent with those of a previous report, which observed that defects in B lymphopoiesis are modulated by MT1-MMP–mediated cleavage of Dll-1 on BM stromal cells.[45] Impaired BM myelopoiesis was found in MT1-MMP–deficient mice, regardless of the fact that G-CSF expression was normal. Factors such as KitL and SDF-1α have also been implicated in myelopoiesis, and therefore might be at least partially responsible for the observed phenotype.

In addition, in vivo administration of KitL and SDF-1α rescued the pancytopenia in MT1-MMP–deficient mice. As both growth factors can increase the egress and mobilization of mature hematopoietic cells, but also can promote hematopoietic cell differentiation, the restoration of PB counts in MT1-MMP–deficient mice could be because of improved hematopoietic cell migration and/or differentiation. We confirmed data by Vagima et al demonstrating that MT1-MMP is expressed on hematopoietic progenitor cells.[21] This group showed that MT1-MMP is required for G-CSF–mediated hematopoietic progenitor cell mobilization.

SDF-1α is required for the maintenance of BM HSCs and is expressed by both perivascular and endosteal cells.[11,13] Deficits in the maintenance of the HSC pool in the absence of CXCR4 are HSC autonomous. Indeed, we could show that MT1-MMP deficiency altered SDF-1α/CXCL12-CXCR4 signaling and impaired the stem cell pool.

Our studies on the role of MT1-MMP in hematopoietic niche/stromal cells provide the rationale for further exploration of MT1-MMP in other hypoxic niches, for example, the cancer niche or the "ischemia-associated niche," as MT1-MMP seems to control the hematopoietic cell response in those diseases by controlling cytokine production.

Acknowledgments

The authors thank the FACS core facility in the Institute of Medical Science (University of Tokyo) for their help. They also thank Dr Hideo Ema for critical advice. Stephanie C. Napier kindly provided editorial assistance to the authors during the preparation of this manuscript. Pauline O'Grady edited the manuscript.

This work was supported by grants from the Japan Society for the Promotion of Science and Grants-in-Aid for Scientific Research from the Ministry of Education, Culture, Sports, Science and Technology (MEXT; K.H. and B.H.); a Grant-in-Aid for Scientific Research on Priority Areas from the MEXT (K.H.); the Mitsubishi Pharma Research Foundation (K.H.); a Grant-in-Aid for Scientific Research on Innovative Areas from the MEXT (B.H.); and the Program for Improvement of the Research Environment for Young Researchers (B.H.) funded by the Special Coordination Funds for Promoting Science and Technology of the MEXT, Japan. In addition, this work was supported by grants from ENSHIN Medical Research Foundation, from Kyowa Hakko Kirin Co Ltd, and from Daiichi Sankyo Company Ltd (K.H.).

Authorship

Contribution: C.N., B.H., and K.H. designed and performed experiments, analyzed and interpreted data, and wrote the manuscript; K.K., Y.T., I.G., A.S., M.O.-K., Y.M., M.N., T.S., N.K., T.K., and S.K.-K. participated in performing experiments, data analysis, and discussion; M.S. and H.N. interpreted data; and H.N., B.H., and K.H. assisted with experimental design and manuscript writing.

Conflict-of-interest disclosure: The authors declare no competing financial interests.

Correspondence: Koichi Hattori, MD, PhD, Center for Stem Cell Biology and Regenerative Medicine, Institute of Medical Science at the University of Tokyo, 4-6-1, Shirokanedai, Minato-ku, Tokyo 108-8639, Japan; e-mail: khattori@ims.u-tokyo.ac.jp.

References

1. Schofield R. The relationship between the spleen colony-forming cell and the haemopoietic stem cell. *Blood Cells.* 1978;4(1-2):7-25.
2. Adams GB, Chabner KT, Alley IR, et al. Stem cell engraftment at the endosteal niche is specified by the calcium-sensing receptor. *Nature.* 2006; 439(7076):599-603.
3. Takubo K, Goda N, Yamada W, et al. Regulation of the HIF-1alpha level is essential for hematopoietic stem cells. *Cell Stem Cell.* 2010;7(3):391-402.
4. Jang YY, Sharkis SJ. A low level of reactive oxygen species selects for primitive hematopoietic stem cells that may reside in the low-oxygenic niche. *Blood.* 2007;110(8):3056-3063.
5. Adelman DM, Maltepe E, Simon MC. Multilineage embryonic hematopoiesis requires hypoxic ARNT activity. *Genes Dev.* 1999;13(19):2478-2483.
6. Scortegagna M, Morris MA, Oktay Y, Bennett M, Garcia JA. The HIF family member EPAS1/HIF-2alpha is required for normal hematopoiesis in mice. *Blood.* 2003;102(5):1634-1640.
7. Rey S, Semenza GL. Hypoxia-inducible factor-1-dependent mechanisms of vascularization and vascular remodelling. *Cardiovasc Res.* 2010; 86(2):236-242.
8. Hattori K, Heissig B, Wu Y, et al. Placental growth factor reconstitutes hematopoiesis by recruiting VEGFR1(+) stem cells from bone-marrow microenvironment. *Nat Med.* 2002;8(8):841-849.
9. Arai F, Hirao A, Ohmura M, et al. Tie2/angiopoietin-1 signaling regulates hematopoietic stem cell quiescence in the bone marrow niche. *Cell.* 2004; 118(2):149-161.
10. Heissig B, Hattori K, Dias S, et al. Recruitment of stem and progenitor cells from the bone marrow

niche requires MMP-9 mediated release of kit-ligand. *Cell.* 2002;109(5):625-637.

11. Kollet O, Dar A, Shivtiel S, et al. Osteoclasts degrade endosteal components and promote mobilization of hematopoietic progenitor cells. *Nat Med.* 2006;12(6):657-664.
12. Ehninger A, Trumpp A. The bone marrow stem cell niche grows up: mesenchymal stem cells and macrophages move in. *J Exp Med.* 2011;208(3): 421-428.
13. Sugiyama T, Kohara H, Noda M, Nagasawa T. Maintenance of the hematopoietic stem cell pool by CXCL12-CXCR4 chemokine signaling in bone marrow stromal cell niches. *Immunity.* 2006; 25(6):977-988.
14. Tokoyoda K, Egawa T, Sugiyama T, Choi BI, Nagasawa T. Cellular niches controlling B lymphocyte behavior within bone marrow during development. *Immunity.* 2004;20(6):707-718.
15. Egawa T, Kawabata K, Kawamoto H, et al. The earliest stages of B cell development require a chemokine stromal cell-derived factor/pre-B cell growth-stimulating factor. *Immunity.* 2001;15(2): 323-334.
16. Fleming HE, Paige CJ. Pre-B cell receptor signaling mediates selective response to IL-7 at the pro-B to pre-B cell transition via an ERK/MAP kinase-dependent pathway. *Immunity.* 2001; 15(4):521-531.
17. Peschon JJ, Morrissey PJ, Grabstein KH, et al. Early lymphocyte expansion is severely impaired in interleukin 7 receptor-deficient mice. *J Exp Med.* 1994;180(5):1955-1960.
18. von Freeden-Jeffry U, Vieira P, Lucian LA, McNeil T, Burdach SE, Murray R. Lymphopenia in interleukin (IL)-7 gene-deleted mice identifies IL-7 as a nonredundant cytokine. *J Exp Med.* 1995; 181(4):1519-1526.
19. Heissig B, Lund LR, Akiyama H, et al. The plasminogen fibrinolytic pathway is required for hematopoietic regeneration. *Cell Stem Cell.* 2007; 1(6):658-670.
20. Lehti K, Rose NF, Valavaara S, Weiss SJ, Keski-Oja J. MT1-MMP promotes vascular smooth muscle dedifferentiation through LRP1 processing. *J Cell Sci.* 2009;122:126-135.
21. Vagima Y, Avigdor A, Goichberg P, et al. MT1-MMP and RECK are involved in human CD34+ progenitor cell retention, egress, and mobilization. *J Clin Invest.* 2009;119(3):492-503.
22. Chun TH, Hotary KB, Sabeh F, Saltiel AR, Allen ED, Weiss SJ. A pericellular collagenase directs the 3-dimensional development of white adipose tissue. *Cell.* 2006;125(3):577-591.
23. Sakamoto T, Seiki M. A membrane protease regulates energy production in macrophages by activating hypoxia-inducible factor-1 via a non-proteolytic mechanism. *J Biol Chem.* 2010; 285(39):29951-29964.
24. Sakamoto T, Seiki M. Cytoplasmic tail of MT1-MMP regulates macrophage motility independently from its protease activity. *Genes Cells.* 2009;14(5):617-626.
25. Itoh Y, Seiki M. MT1-MMP: a potent modifier of pericellular microenvironment. *J Cell Physiol.* 2006;206(1):1-8.
26. Hotary KB, Allen ED, Brooks PC, Datta NS, Long MW, Weiss SJ. Membrane type I matrix metalloproteinase usurps tumor growth control imposed by the three-dimensional extracellular matrix. *Cell.* 2003;114(1):33-45.
27. Seiki M. Membrane-type 1 matrix metalloproteinase: a key enzyme for tumor invasion. *Cancer Lett.* 2003;194(1):1-11.
28. Holmbeck K, Bianco P, Caterina J, et al. MT1-MMP-deficient mice develop dwarfism, osteopenia, arthritis, and connective tissue disease due to inadequate collagen turnover. *Cell.* 1999;99(1): 81-92.
29. Hattori K, Heissig B, Tashiro K, et al. Plasma elevation of stromal cell-derived factor-1 induces mobilization of mature and immature hematopoietic progenitor and stem cells. *Blood.* 2001; 97(11):3354-3360.
30. Taniwaki K, Fukamachi H, Komori K, et al. Stroma-derived matrix metalloproteinase (MMP)-2 promotes membrane type 1-MMP-dependent tumor growth in mice. *Cancer Res.* 2007;67(9):4311-4319.
31. Mendez-Ferrer S, Michurina TV, Ferraro F, et al. Mesenchymal and haematopoietic stem cells form a unique bone marrow niche. *Nature.* 2010; 466(7308):829-834.
32. Maiese K, Chong ZZ, Shang YC. Raves and risks for erythropoietin. *Cytokine Growth Factor Rev.* 2008;19(2):145-155.
33. Munugalavadla V, Kapur R. Role of c-Kit and erythropoietin receptor in erythropoiesis. *Crit Rev Oncol Hematol.* 2005;54(1):63-75.
34. Wang W, Horner DN, Chen WL, Zandstra PW, Audet J. Synergy between erythropoietin and stem cell factor during erythropoiesis can be quantitatively described without co-signaling effects. *Biotechnol Bioeng.* 2008;99(5):1261-1272.
35. Socolovsky M, Nam H, Fleming MD, Haase VH, Brugnara C, Lodish HF. Ineffective erythropoiesis in Stat5a(−/−)5b(−/−) mice due to decreased survival of early erythroblasts. *Blood.* 2001; 98(12):3261-3273.
36. Link A, Vogt TK, Favre S, et al. Fibroblastic reticular cells in lymph nodes regulate the homeostasis of naive T cells. *Nat Immunol.* 2007;8(11):1255-1265.
37. Webb JD, Coleman ML, Pugh CW. Hypoxia, hypoxia-inducible factors (HIF), HIF hydroxylases and oxygen sensing. *Cell Mol Life Sci.* 2009; 66(22):3539-3554.
38. Mahon PC, Hirota K, Semenza GL. FIH-1: a novel protein that interacts with HIF-1alpha and VHL to mediate repression of HIF-1 transcriptional activity. *Genes Dev.* 2001;15(20):2675-2686.
39. Kasper LH, Boussouar F, Boyd K, et al. Two transactivation mechanisms cooperate for the bulk of HIF-1-responsive gene expression. *EMBO J.* 2005;24(22):3846-3858.
40. McQuibban GA, Butler GS, Gong JH, et al. Matrix metalloproteinase activity inactivates the CXC chemokine stromal cell-derived factor-1. *J Biol Chem.* 2001;276(47):43503-43508.
41. Ceradini DJ, Kulkarni AR, Callaghan MJ, et al. Progenitor cell trafficking is regulated by hypoxic gradients through HIF-1 induction of SDF-1. *Nat Med.* 2004;10(8):858-864.
42. Forsythe JA. Activation of vascular endothelial growth factor gene transcription by hypoxia-inducible factor 1. *Mol Cell Biol.* 1996;16(9):4604-4613.
43. Simon MP, Tournaire R, Pouyssegur J. The angiopoietin-2 gene of endothelial cells is up-regulated in hypoxia by a HIF binding site located in its first intron and by the central factors GATA-2 and Ets-1. *J Cell Physiol.* 2008;217(3): 809-818.
44. Robey E, Chang D, Itano A, et al. An activated form of notch influences the choice between CD4 and CD8 T cell lineages. *Cell.* 1996;87(3):483-492.
45. Jin G, Zhang F, Chan KM, et al. MT1-MMP cleaves Dll1 to negatively regulate Notch signalling to maintain normal B-cell development. *EMBO J.* 2011;30:2281-2293.
46. Schmitt TM, Ciofani M, Petrie HT, Zuniga-Pflucker JC. Maintenance of T cell specification and differentiation requires recurrent notch receptor-ligand interactions. *J Exp Med.* 2004;200(4): 469-479.
47. Namen AE, Lupton S, Hjerrild K, et al. Stimulation of B-cell progenitors by cloned murine interleukin-7. *Nature.* 1988;333(6173):571-573.
48. Rolink A, Streb M, Nishikawa S, Melchers F. The c-kit-encoded tyrosine kinase regulates the proliferation of early pre-B cells. *Eur J Immunol.* 1991; 21(10):2609-2612.
49. Sudo T, Nishikawa S, Ohno N, Akiyama N, Tamakoshi M, Yoshida H. Expression and function of the interleukin 7 receptor in murine lymphocytes. *Proc Natl Acad Sci U S A.* 1993;90(19): 9125-9129.
50. Nagasawa T, Hirota S, Tachibana K, et al. Defects of B-cell lymphopoiesis and bone-marrow myelopoiesis in mice lacking the CXC chemokine PBSF/SDF-1. *Nature.* 1996;382(6592):635-638.

blood

2012 120: 1299-1308
Prepublished online June 21, 2012;
doi:10.1182/blood-2012-03-417881

Induced pluripotent stem cells from CINCA syndrome patients as a model for dissecting somatic mosaicism and drug discovery

Takayuki Tanaka, Kazutoshi Takahashi, Mayu Yamane, Shota Tomida, Saori Nakamura, Koichi Oshima, Akira Niwa, Ryuta Nishikomori, Naotomo Kambe, Hideki Hara, Masao Mitsuyama, Nobuhiro Morone, John E. Heuser, Takuya Yamamoto, Akira Watanabe, Aiko Sato-Otsubo, Seishi Ogawa, Isao Asaka, Toshio Heike, Shinya Yamanaka, Tatsutoshi Nakahata and Megumu K. Saito

Blood (print ISSN 0006-4971, online ISSN 1528-0020), is published weekly by the American Society of Hematology, 2021 L St, NW, Suite 900, Washington DC 20036.

Induced pluripotent stem cells from CINCA syndrome patients as a model for dissecting somatic mosaicism and drug discovery

Takayuki Tanaka,[1] Kazutoshi Takahashi,[1] Mayu Yamane,[1] Shota Tomida,[1] Saori Nakamura,[1] Koichi Oshima,[1] Akira Niwa,[1] Ryuta Nishikomori,[2] Naotomo Kambe,[3] Hideki Hara,[4] Masao Mitsuyama,[4] Nobuhiro Morone,[5] John E. Heuser,[5] Takuya Yamamoto,[1] Akira Watanabe,[1] Aiko Sato-Otsubo,[6] Seishi Ogawa,[6] Isao Asaka,[1] Toshio Heike,[2] Shinya Yamanaka,[1,5,7,8] Tatsutoshi Nakahata,[1,2] and Megumu K. Saito[1]

[1]Center for iPS Cell Research and Application and [2]Department of Pediatrics, Kyoto University, Kyoto, Japan; [3]Department of Dermatology, Chiba University Graduate School of Medicine, Chiba, Japan; [4]Department of Microbiology and [5]Institute for Integrated Cell-Material Sciences, Kyoto University, Kyoto, Japan; [6]Cancer Genomics Project, University of Tokyo, Tokyo, Japan; [7]Yamanaka iPS Cell Special Project, Japan Science and Technology Agency, Kawaguchi, Japan; and [8]Gladstone Institute of Cardiovascular Disease, San Francisco, CA

Chronic infantile neurologic cutaneous and articular (CINCA) syndrome is an IL-1–driven autoinflammatory disorder caused mainly by *NLRP3* mutations. The pathogenesis of CINCA syndrome patients who carry *NLRP3* mutations as somatic mosaicism has not been precisely described because of the difficulty in separating individual cells based on the presence or absence of the mutation. Here we report the generation of *NLRP3*-mutant and nonmutant-induced pluripotent stem cell (iPSC) lines from 2 CINCA syndrome patients with somatic mosaicism, and describe their differentiation into macrophages (iPS-MPs). We found that mutant cells are predominantly responsible for the pathogenesis in these mosaic patients because only mutant iPS-MPs showed the disease relevant phenotype of abnormal IL-1β secretion. We also confirmed that the existing anti-inflammatory compounds inhibited the abnormal IL-1β secretion, indicating that mutant iPS-MPs are applicable for drug screening for CINCA syndrome and other NLRP3-related inflammatory conditions. Our results illustrate that patient-derived iPSCs are useful for dissecting somatic mosaicism and that *NLRP3*-mutant iPSCs can provide a valuable platform for drug discovery for multiple NLRP3-related disorders. (*Blood*. 2012;120(6):1299-1308)

Introduction

Chronic infantile neurologic cutaneous and articular syndrome (CINCA syndrome; MIM #607715) is a dominantly inherited autoinflammatory disease characterized by systemic inflammation with an urticaria-like rash, neurologic manifestations, and arthropathy.[1] *NLRP3* mutation is the first and so far the only identified mutation that is responsible for CINCA syndrome.[2,3] *NLRP3* is expressed mainly in myelomonocytic lineage cells and chondrocytes[3] and acts as an intracellular sensor of danger signals from various cellular insults. In normal macrophages, a first stimulus, such as lipopolysaccharide (LPS), induces the synthesis of NLRP3 and the biologically inactive proIL-1β.[4] A second stimulus, such as ATP, enhances the assembly of a protein complex called the NLRP3-inflammasome.[5] The inflammasome contains caspase1, which executes the proteolytic maturation and secretion of IL-1β. Although normal monocytes/macrophages show no or limited IL-1β secretion in response to LPS stimulation alone, CINCA patients' cells exhibit robust IL-1β secretion because the mutant NLRP3-inflammasome is autoactivated without the need for any second stimulus.[6] It is therefore thought that the manifestations of CINCA syndrome are predominantly caused by the excessive secretion of the proinflammatory cytokine, IL-1β, and this concept is supported by the efficacy of an IL-1 receptor antagonist (IL-1Ra) for decreasing most of the symptoms.[7] However, because IL-1Ra treatment does not seem to ameliorate the characteristic arthropathy of cartilage overgrowth and joint contraction,[8] a more specific therapeutic approach that directly modulates the NLRP3-inflammasome is desired.

Although approximately half of CINCA patients carry heterozygous gain-of-function mutations of the *NLRP3* gene,[2,3] 30% to 40% of all patients have mutations in *NLRP3* in only a small number of somatic cells.[9,10] Because the population of mutant cells is relatively small (4.2%-35.8% in blood cells), it remains controversial whether the small fraction of *NLRP3*-mutated cells actually causes the strong autoinflammation observed in CINCA patients, or whether the *NLRP3* mutations found in mosaic patients are just a bystander, with all cells carrying an unknown mutation of another gene that causes the disease.[11]

Somatic mosaicism refers to the presence of more than 1 genetically distinct cell population in a single person, and has been identified in patients with various diseases.[12,13] The relevance of somatic mosaicism to the onset of diseases has been suggested mainly through sequence-based approaches. However, direct evidence that a cell population with a distinct genetic property shows disease-specific characteristics is lacking because it has been impossible to separately extract individual live cells from affected tissues to assess their biologic characteristics. Regarding hematopoietic disorders in which mutant cells show decreased expression of a certain protein, genetic heterogeneity caused by somatic mutations was detected by flow cytometry after intracellular staining,[14-16] but sorting out alive mutant and nonmutant cells for evaluating biologic property has been impossible.

Submitted March 27, 2012; accepted May 29, 2012. Prepublished online as *Blood* First Edition paper, June 21, 2012; DOI 10.1182/blood-2012-03-417881.

The online version of this article contains a data supplement.

The publication costs of this article were defrayed in part by page charge payment. Therefore, and solely to indicate this fact, this article is hereby marked "advertisement" in accordance with 18 USC section 1734.

Induced pluripotent stem cells (iPSCs) are pluripotent cell lines directly reprogrammed from somatic cells.[17] Patient-derived iPSCs can provide somatic cells, which cannot be directly obtained from patients, and this discovery has led to the development of a new field of disease modeling (reviewed by Grskovic et al[18]). In addition, iPSC technology has another interesting characteristic that each iPSC clone originates from a single cell,[19] which may make it possible to obtain genetically different iPSC clones from a person.

In this study, we established mutant and nonmutant iPSC lines from the same patients by deriving iPSCs from patients carrying a mutation of an autosomal gene as somatic mosaicism. By analyzing the disease-relevant characteristic of IL-1β secretion, we demonstrated that mutant macrophages are mainly responsible for the disease phenotype in the mosaic patients. Moreover, using a robust differentiation protocol to generate macrophages and purifying them by their surface marker expression, we showed that drug candidates inhibit the IL-1β secretion from mutant macrophages. Our data prove the usefulness of iPSC technology both for dissecting somatic mosaicism and as a platform for drug discovery of multiple NLRP3-related inflammatory diseases.

Methods

Human iPSC generation

We obtained skin biopsy specimens from 2 independent patients (patient 1, CIRA188Ai; and patient 2, CIRA086Ai). This study was approved by Ethics Committee of Kyoto University, and informed consent was obtained from both the patients and their guardians in accordance with the Declaration of Helsinki. We expanded the fibroblasts in DMEM (Nacalai Tesque) containing 10% FBS (Invitrogen) and 0.5% penicillin and streptomycin (Invitrogen). Generation of iPS cells was performed as described previously.[17] In brief, we introduced *OCT3/4*, *SOX2*, *KLF4*, and *c-MYC* using ecotropic retroviral transduction into fibroblasts expressing the mouse *Slc7a1* gene. Six days after transduction, the cells were harvested and replated onto mitotically inactivated SNL feeder cells. The next day, we replaced the medium with Primate ES cell medium (ReproCELL) supplemented with 4 ng/mL bFGF (Wako). Three weeks after this period, individual colonies were isolated and expanded. Cell culture was performed under 37°C, with 5% CO_2 and 21% O_2 unless otherwise stated. Cells were examined using Olympus CKX41 inverted microscope equipped with Nikon Digital Sight DS-L2 camera. A UPlan FLN 4×/0.13 objective (Nikon) was used for image acquisition.

Genetic analysis

Genomic DNA from either fibroblasts or iPSCs was isolated. The PCR product of exon 3 of *NLRP3* was sequenced directly or after subcloning with a TOPO TA cloning kit (Invitrogen), using an ABI 3100 sequencer (Applied Biosystems). For pyrosequencing, the PCR product of exon 3 of *NLRP3* was analyzed by PyroMarkQ96ID (QIAGEN).

RNA isolation and quantitative PCR for *NANOG* and the transgene

Total RNA was purified with the Trizol reagent (Invitrogen) and treated with a Turbo DNA-free kit (Ambion) to remove genomic DNA contamination. A total of 1 μg of total RNA was used for a reverse transcription reaction with ReverTraAce-α (Toyobo) and the dT_{20} primer, according to the manufacturer's instructions. Quantitative PCR was performed on the 7900HT Fast Real-Time PCR System (Applied Biosystems) with SYBR Premix ExTaqII (Takara). The primer sequences are described in supplemental Table 4 (available on the *Blood* Web site; see the Supplemental Materials link at the top of the online article).

Southern blotting

Genomic DNA (5 μg) was digested with BglII and ScaI overnight. The digested DNA fragments were separated on 1% agarose gels and were transferred to a nylon membrane (GE Healthcare). The membrane was incubated with a digoxigenin (DIG)–labeled human *cMYC* DNA probe in DIG Easy Hyb buffer (Roche Diagnostics) at 42°C overnight with constant agitation. After washing, an alkaline phosphatase-conjugated anti-DIG antibody (1:10 000; Roche Diagnostics) was added to a membrane. Signals were obtained using CDP-star (Roche Diagnostics) and detected by an LAS4000 imaging system.

Teratoma formation

Approximately 2×10^6 cells were injected subcutaneously into the dorsal flank of immunocompromised NOD/scid/γc^{null} mice (Central Institute for Experimental Animals). Masses were excised 8 to 10 weeks after injection and fixed with PBS containing 4% paraformaldehyde. Paraffin-embedded tissues were sliced and stained with hematoxylin and eosin. Slides were examined using BIOREVO BZ-9000 (KEYENCE). A PlanApo 20×/0.75 objective (Nikon) and BZ-II Viewer software (KEYENCE) were used for image acquisition.

In vitro differentiation into macrophages

Undifferentiated human embryonic stem cell (ESC) and iPSC lines were cultured on mitotically inactivated SNL feeder cells with Primate ES cell medium supplemented with 4 ng/mL bFGF. During the differentiation of the cells into macrophages, cells were cultured under 37°C, with 5% CO_2 and 5% O_2. On day 0, the iPSCs were plated at a ratio of 1:15 onto a mitotically inactivated OP9 feeder layer on 100-mm cell culture plates in α-MEM (Invitrogen) containing 10% FBS and 1% Antibiotic-Antimycotic (Invitrogen) supplemented with 50 ng/mL VEGFα (R&D Systems). On day 5, the medium was changed. On day 10, the differentiating iPSCs were collected by trypsinization, and Tra-1-85$^+$ CD34$^+$ and KDR$^+$ hematopoietic progenitors were sorted on a FACSAria II instrument (BD Biosciences). The progenitors were plated at 2×10^4 cells on another mitotically inactivated OP9 feeder layer on 100-mm cell culture plates or at 3×10^3 cells/well in 6-well cell culture plates in α-MEM containing 10% FBS and 1% Antibiotic-Antimycotic supplemented with 50 ng/mL IL-3, 50 ng/mL stem cell factor, 10 ng/mL thrombopoietin, 50 ng/mL Flt-3 ligand, and 50 ng/mL M-CSF (all R&D Systems). On day 18, the medium was changed. On day 26, differentiating cells were collected with Accumax (Innovative Cell Technologies), and CD14$^+$ iPSC-derived macrophages were purified on an autoMACSpro instrument (Miltenyi Biotec).

Peripheral blood mononuclear cells (PBs) were obtained from healthy volunteers, and CD14$^+$ monocytes were purified on the autoMACSpro instrument. For macrophage differentiation, 5×10^5 monocytes were plated in 6-well cell culture plates in RPMI 1640 (Sigma-Aldrich) containing 10% FBS and 1% Antibiotic-Antimycotic supplemented with 50 ng/mL M-CSF. On day 5, the adherent cells were collected with Accumax, and CD14$^+$ blood-derived macrophages (B-MPs) were purified on the autoMACSpro instrument. May-Giemsa–stained slides were examined using BIOREVO BZ-9000. A PlanApo 40×/0.95 objective (Nikon) and BZ-II Viewer software were used for image acquisition.

FACS analysis

Hematopoietic marker expression was evaluated on a MACSQuant Analyzer (Miltenyi Biotec). Primary antibodies Tra-1-85-FITC (R&D Systems), CD34-PE (Beckman Coulter), KDR–AlexaFluor-647 (BioLegend), CD45-PE (BD Biosciences PharMingen), and CD14-APC (Beckman Coulter) were used.

Immunocytochemistry

For immunocytochemistry, cells were fixed with PBS containing 4% paraformaldehyde for 5 minutes, permeabilized in PBS containing 0.1% Tween 20 for 5 minutes, and blocked in PBS containing 3% BSA for 10 minutes, all at room temperature. The primary antibody was for CD68 (1:50; Santa Cruz Biotechnology), and the secondary antibody was Cy3-conjugated

AffiniPure Donkey Anti–Mouse IgG (1:100; Jackson ImmunoResearch Laboratories). Nuclei were stained with 1 μg/mL Hoechst 33342 (Invitrogen). Cells were examined using BIOREVO BZ-9000. A Plan Fluor DL 10×/0.30 Ph1 objective (Nikon) and BZ-II Viewer software were used for image acquisition.

Electron microscopy

The 5×10^4 macrophages in 20 μL suspension were placed on the poly-L-lysine treated, carbon-coated sapphire disks (3 mm in diameter) and incubated for 30 minutes at 37°C with 5% CO_2. The cell-adsorbed disk was then subjected to chemical fixation with 2.5% glutaraldehyde in NaHCa buffer (100mM NaCl, 30mM HEPES, 2mM $CaCl_2$, adjusted at pH 7.4 with NaOH). These specimens were postfixed with 1% osmium and 1.5% $K_4Fe(CN)_6$ in 0.1M PBS buffer, washed, dehydrated with a series of ethanol, and embedded in Epoxy resin (TAAB EPON812). After the polymerization at 70°C, the ultra-sections (70 nm) obtained by Ultramicrotome (Leica FC6) were mounted in EM grids, stained with uranyl acetate/lead citrate, and then observed by conventional TEM (JEOL JEM1400).

PCR and microarray analysis of macrophages

Total RNA was column-purified with the RNeasy kit (QIAGEN) and treated with RNase-free DNase (QIAGEN). A total of 20 ng of total RNA was reverse transcribed into cDNA using random primers and the Sensiscript RT Kit (QIAGEN). Quantitative PCR was performed on a StepOne Plus Real-Time PCR System (Applied Biosystems) with TaqMan Gene Expression Master Mix (Applied Biosystems). The primer sequences are described in supplemental Table 4. For the microarray analysis, RNA probes were hybridized to SurePrint G3 Human GE 8×60K Microarrays (Agilent Technologies) according to the manufacturer's protocols. Microarrays were scanned, and the data were analyzed using the GeneSpring GX Version 11 software program (Agilent Technologies). The complete dataset from this analysis is available at the NCBI Gene Expression Omnibus using accession no. GSE38626.

LM infection

Listeria monocytogenes EGD (LM) were grown in brain heart infusion broth (Eieken Chemical), washed, suspended in PBS supplemented with 10% glycerol, and stored in aliquots at −80°C. Macrophages were seeded into an 8-well chamber slide at 2×10^5 cells/well in RPMI containing 10% FBS and then infected with bacteria at a multiplicity of infection of 10 for 60 minutes at 37°C. Cells were cultured for further 1 or 5 hours in the presence of 5 μg/mL gentamicin. The cells were fixed in 4% paraformaldehyde and incubated with PBS containing 10% Blocking One (Nacalai Tesque) and 0.1% saponin. F-actin and nuclei were visualized by staining with Alexa-488-phalloidin (Invitrogen) and 4′,6-diamidino-2-phenylindole (Dojindo), respectively. The bacteria were stained by treatment with a goat anti-*Listeria* polyclonal antibody (Kirkegaard & Perry Laboratories) and then with the Alexa 546 anti–goat IgG antibody (Invitrogen). Slides were examined using BIOREVO BZ-9000. A PlanApo_VC 100×H/1.40 objective (Nikon) and BZ-II Viewer software were used for image acquisition, and BZ-II Analyzer (KEYENCE) was used for image processing. Immunofluorescence was evaluated with the IN Cell Analyzer 2000, and samples were analyzed with the IN Cell Developer Toolbox Version 1.8 software program (GE Healthcare).

Cytokine secretion from macrophages

Purified iPS-MPs or B-MPs were seeded at the indicated counts per well or 5×10^4 cells/well unless otherwise stated in 96-well cell culture plates in RPMI 1640 containing 10% FBS and 1% Antibiotic-Antimycotic. Cells were cultured for 2 hours in the presence or absence of inhibitors. The plates were centrifuged at 300*g* for 10 minutes; then the medium was changed. Cells were cultured for 4 hours in the presence of LPS or recombinant human IL-1β. LPS concentration was 1 μg/mL unless otherwise stated. After the 30 minute or 1-hour culture after the addition of 1mM ATP (Sigma-Aldrich), we collected the supernatants and cell lysates. As second signal stimulants, we also used 500 μg/mL silica crystals (U.S. silica) for 1 hour, or 100 μg/mL monosodium urate crystals (Sigma-Aldrich) for 3 hours. For the supernatant transfer experiments, we harvested the supernatant from the wells of mutant or wild-type iPS-MPs, which were stimulated with LPS for 4 hours. After centrifugation, we transferred the supernatants to the wells of other iPS-MPs and cultured them for another 4 hours. The cytokine concentration of the supernatants was determined using a Th1/Th2 11plex FlowCytomix Kit (Bender MedSystems) following the manufacturer's instructions. Reagents were purchased as follows: CA074Me (Calbiochem), IL-1Ra (R&D Systems), oxidized ATP (oATP; Sigma-Aldrich), pyridoxalphosphate-6-azophenyl-2′,4′-disulphonic acid (PPADS; Sigma-Aldrich), cycloheximide (Sigma-Aldrich), MG132 (Calbiochem), Bay11-7082 (Sigma-Aldrich), and Ac-YVAD-CHO (Calbiochem).

LDH secretion assay

The lactate dehydrogenase (LDH) concentration of the supernatants of iPS-MPs after a 4-hour culture with LPS was determined with an LDH Cytotoxicity Detection kit (Takara) following the manufacturer's instructions.

Statistical analysis

The data were processed using the SPSS Statistics Version 18 software package. The values are reported as the mean ± SEM. Comparisons between groups were performed using the unpaired Student *t* test. $P < .05$ was considered statistically significant.

Results

Establishment and characterization of iPSCs

Dermal fibroblasts were obtained from 2 male CINCA patients who had mutations of *NLRP3* as somatic mosaicism. Both patients had nonsynonymous point mutations in the *NLRP3* coding region. The fibroblasts from patients 1 and 2 contained 34% and 9.8% mutant cells, respectively (Figure 1A; supplemental Figure 1A). These fibroblasts were reprogrammed to iPSCs after transduction with retroviral vectors encoding *OCT3/4*, *SOX2*, *KLF4*, and cMYC.[17] Twelve of the 28 isolated clones from patient 1, and 3 of 30 clones from patient 2 had a heterozygous mutation of the *NLRP3* gene, whereas the rest of the clones were wild-type (Figure 1A; supplemental Figure 1B-C). The frequency of mutants was comparable among blood cells,[9,20] fibroblasts, and iPSCs (Table 1). We randomly selected 3 mutant (M1-M3) and 3 wild-type clones (W1-W3) from patient 1 and 3 mutant (m1-m3) and 3 wild-type clones (w1-w3) from patient 2 for the propagation and subsequent analyses.

All iPSC clones showed a characteristic human ESC-like morphology (Figure 1B), the reactivation of endogenous pluripotency genes (*OCT3/4*, *SOX2*, *NANOG*; Figure 1C-D; supplemental Figure 1D) and the demethylation of the *OCT3/4* promoter regions (supplemental Figure 1E). Transgene expression was rarely detected (Figure 1D; supplemental Figure 1D), and the retroviral integration patterns were confirmed by a Southern blot analysis (Figure 1E; supplemental Figure 1F). All of the iPSC clones maintained a normal karyotype (data not shown). There were neither proviral integration nor copy number changes observed in any of the genes that might affect the function of the NLRP3 inflammasome (supplemental Tables 1 and 2). Genetic identity was proven by a short tandem repeat analysis (supplemental Table 3), and the pluripotency of the iPSC clones was confirmed by the presence of cell derivatives of all 3 germ layers by teratoma formation after injection of undifferentiated iPSCs into immunocompromised NOD/scid/γc^{null} mice (Figure 1F; supplemental Figure 1G).

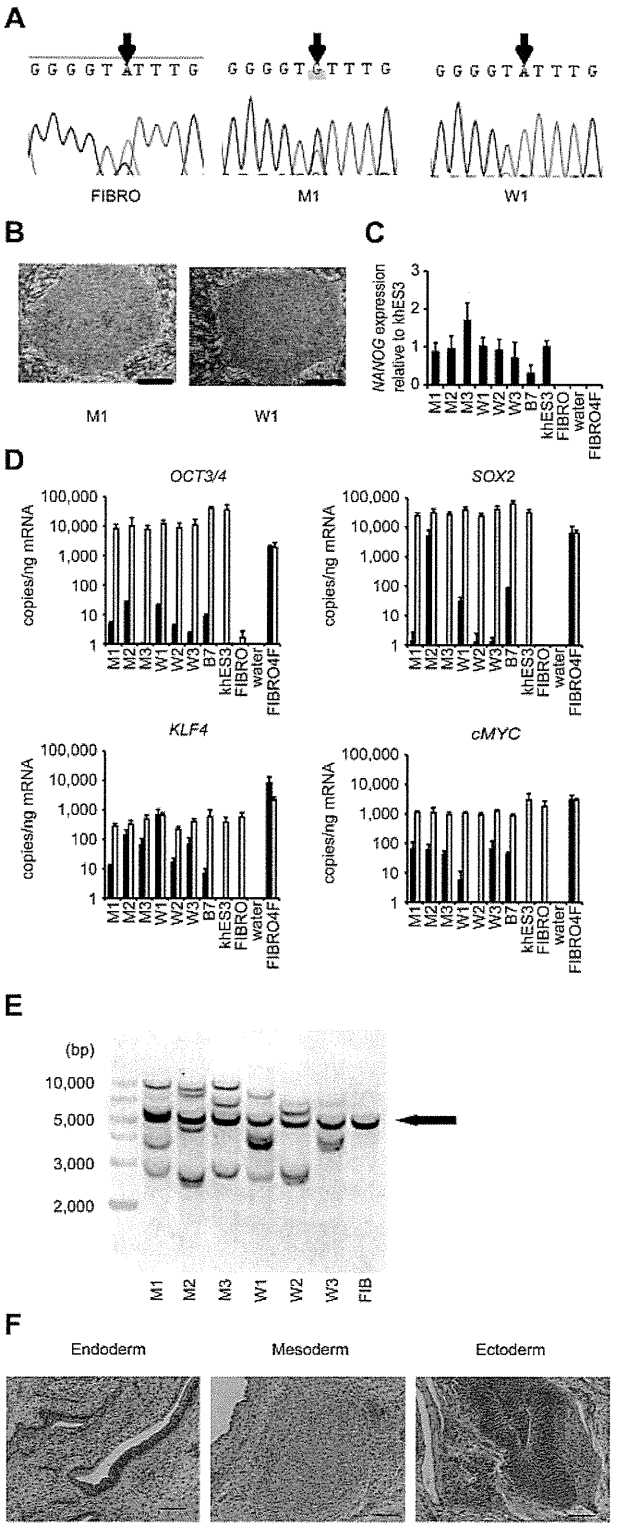

Figure 1. Establishment and characterization of iPSCs. (A) Sequencing of the *NLRP3* 1709 A > G mutation (Y570C) in fibroblasts (FIBRO), mutant iPSCs (M1), and wild-type iPSCs (W1) in patient 1. (B) The morphology of the mutant and wild-type iPSCs. (C) *NANOG* expression in CINCA iPSCs, control iPSCs (B7), control ESCs (khES3), fibroblasts (FIBRO), and fibroblasts transduced with 4 factors (FIBRO4F) normalized to *GAPDH*. n = 3. (D) A quantitative RT-PCR assay for the expression of *OCT3/4*, *SOX2*, *KLF4*, and *cMYC* in iPSCs. One primer set detects only the transgene (in black), and the other primer set detects both the transgene and endogenous gene (in white). n = 3. (E) Retroviral transgene integration analyses. Southern blot analyses were performed with DIG-labeled DNA probes against *c-MYC*. The parental fibroblasts carried a band in common with all of the iPSC lines (arrow). (F) A teratoma derived from a mutant iPSC clone, M1. Scale bars represent 100 μm. Data are mean ± SEM.

Differentiation and characterization of iPSC-derived macrophages

To compare the most prominent features of the disease, we differentiated the patient-derived iPSCs into the monocyte/macrophage lineage using a murine stromal cell line, OP9.[21] After culturing the iPSCs on an OP9 feeder layer for 10 days, we collected KDR$^+$ CD34$^+$ hemangioblasts (Figure 2A). All of the iPSC clones, whether they carried an *NLRP3* mutation or not, differentiated into KDR$^+$ CD34$^+$ progenitors as efficiently as the control ESC or iPSC clones (Figure 2B; supplemental Figure 2A). Adherent CD68$^+$ macrophages emerged after culturing the KDR$^+$ CD34$^+$ cells on another OP9 feeder layer for 16 days (Figure 2C; supplemental Figure 2B). Approximately 80% of the differentiated cells expressed CD14, and magnetic-activated cell sorting increased the purity to almost 100% (Figure 2D). All of the clones we used efficiently produced comparable amounts of iPSC-derived macrophages (iPS-MPs; Figure 2E; supplemental Figure 2C). The iPS-MPs visualized by light and electron microscopy showed a typical morphology, with a high cytoplasm-to-nucleus ratio and cytoplasmic vacuoles (Figure 2F; supplemental Figure 2D). The iPS-MPs showed a global gene expression pattern closer to that of blood-derived macrophages than to the parental iPSC clone (supplemental Figure 2E-F). Both mutant and wild-type iPS-MPs phagocytosed bacteria to the same extent when we infected the cells with Gram-positive LM, an intracellular bacterium that escapes into the cytosol (Figure 2G-H). These data indicate that both the mutant and wild-type iPS-MPs derived from mosaic CINCA patients are indistinguishable based on their gene expression and their phagocytic function.

Elucidation of the pathogenesis of somatic mosaic CINCA syndrome

Monocytes derived from CINCA syndrome patients usually do not spontaneously secrete IL-1β and become active after LPS stimulation.[6] Monocytes or mononuclear cells from untreated CINCA syndrome patients, however, sometimes show an increased synthesis of proIL-1β[2] and secretion of mature IL-1β,[7] even in the absence of LPS stimulation, because they can be activated by persistent inflammation or by the purification procedure. As spontaneous activation complicates the functional analysis, we herein evaluated the IL-1β activation status both before and after the stimulation. We observed that the mRNA expression of *IL1B* was low in unstimulated iPS-MPs and increased to comparable levels in mutant and wild-type iPS-MPs in response to LPS stimulation (supplemental Figure 3A). Similarly, the mRNA level of *NLRP3* was relatively low before LPS stimulation (supplemental Figure 3A). Mature IL-1β was not detectable in the supernatant of the cell culture medium (data not shown). Collectively, these data indicate that the unstimulated iPS-MPs were in an "inactive" state before stimulation.

To identify which iPS-MP clones showed the specific features compatible to patients' monocytes, we evaluated their IL-1β secretion. Although LPS stimulation alone led to IL-1β secretion

Table 1. Mutation frequency among different cell types

Patient no.	Site of mutation	Frequency (%) of mutant cells		
		Whole blood*	Fibroblasts	iPSCs
1	1709A > G(Y570C)	33.3	34.3	42.9
2	919G > A(G307S)	8.5	9.8	10.0

*The frequency in whole blood was reported previously.[9,20]

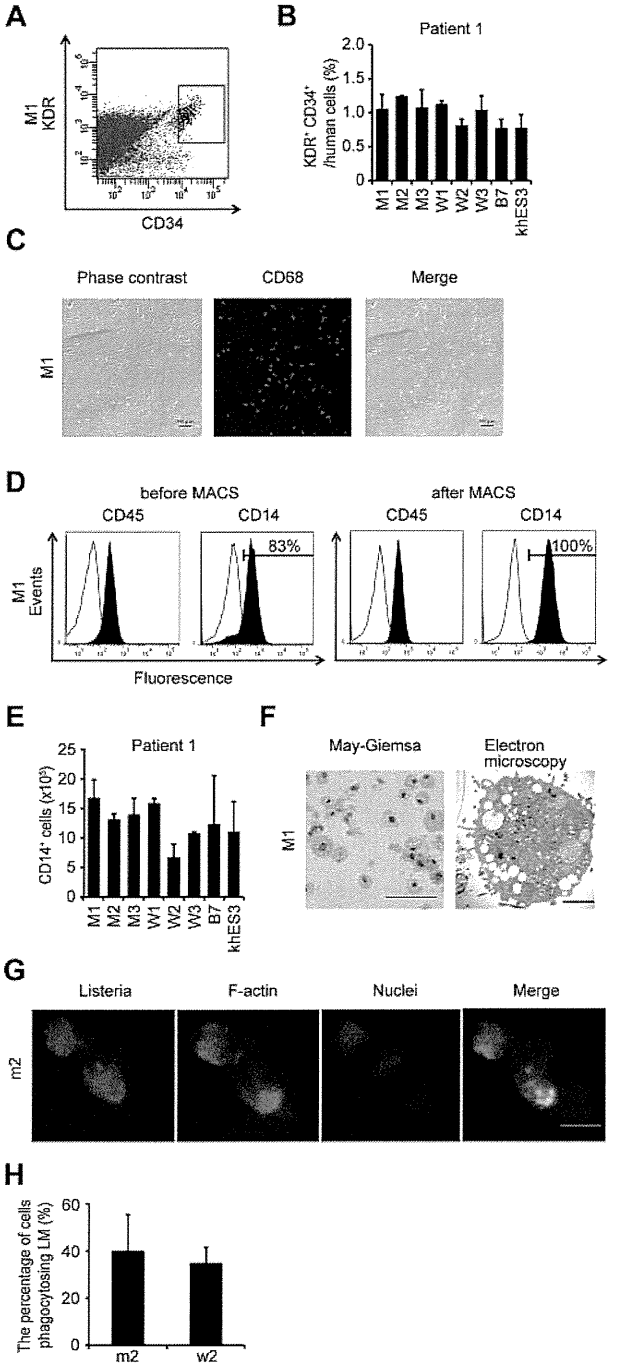

Figure 2. Differentiation and characterization of iPSCs-derived macrophages. (A) KDR$^+$ CD34$^+$ hematopoietic progenitors purified 10 days after differentiation. (B) The percentage of KDR$^+$ CD34$^+$ cells in Tra-1-85$^+$ human cells. n = 3. (C) CD68 immunostaining of macrophages. Scale bars represent 100 μm. (D) The histograms show antibody staining (in black) relative to the isotype-matched controls (in white) for a blood cell marker (CD45), and a macrophage marker (CD14), in cells before (left 2 panels) or after (right 2 panels) magnetic-activated cell sorting purification. (E) CD14$^+$ cell counts obtained from iPSCs plated on an OP9 feeder layer on one 100-mm dish. n = 3. (F) Representative morphology of iPS-MPs evaluated by May-Giemsa staining or transmission electron microscopy. Scale bars represent 100 μm and 2 μm, respectively. (G) The phagocytosis by iPS-MPs after LM infection. The cells were treated with anti-LM antibody, phalloidin, and 4′,6-diamidino-2-phenylindole. Scale bar represents 20 μm. (H) The percentage of iPS-MPs phagocytosing LM was calculated as the average of 9 fields of vision. Data are mean ± SEM.

from the mutant iPS-MPs, the addition of ATP was necessary to induce IL-1β secretion from wild-type iPS-MPs, as it was from either ESC-derived or blood-derived macrophages (Figure 3A). The IL-1β level from mutant iPS-MPs was significantly higher than that from wild-type macrophages, even in the presence of LPS plus ATP. Both groups of macrophages showed similar kinetics in their secretion of other cytokines, such as IL-6 or TNFα (Figure 3A). The results were similar in the iPS-MPs from patient 2 (Figure 3B). Although iPS-MPs showed a similar response at lower LPS concentrations (Figure 3C-D; supplemental Figure 3B-C), no IL-1β secretion was detectable from mutant iPSCs, wild-type iPSCs, or parental fibroblasts in response to stimulation with 1 μg/mL LPS (data not shown). These data demonstrate that the abnormal function of the iPS-MPs is predominantly determined by the *NLRP3* mutation, and not by some unknown genetic alteration(s) prevalent in all cells. We next investigated whether iPS-MPs show pyronecrosis: a pathogen-induced, cathepsin B-dependent, necrosis-like programmed cell death that is characteristically observed in *NLRP3*-mutant monocytes/macrophages.[22,23] When we compared LDH secretion as a marker of membrane rupture, we found that LPS stimulation evoked a significantly higher LDH secretion only from the mutant iPS-MPs, which was inhibited by the cathepsin B inhibitor, CA074Me (Figure 3E).

Despite the low percentage of mutant cells, the clinical manifestation of mosaic CINCA patients is similar to that of patients with a heterozygous mutation.[9,10] We hypothesized that an interaction between the mutant and wild-type macrophages leads to exacerbation of the inflammation. To test this hypothesis, we modeled a mosaic condition by coculturing mutant and wild-type cells. After stimulating mutant iPS-MPs with LPS in separate cultures or in cocultures with wild-type counterparts, we determined the IL-1β level in the supernatant. We found that the IL-1β secretion significantly increased after coculture (Figure 4A; supplemental Figure 4A). Although increasing the cell concentration raised the total amount of the IL-1β secretion from mutants, it did not accelerate the IL-1β secretion per cell from mutant iPS-MPs or enhance the secretion from wild-type macrophages (Figure 4B). To determine the ratio of mutant/wild-type cells at which the additional IL-1β secretion is most enhanced, we changed the ratio using a fixed number of mutant iPS-MPs and increasing the number of wild-type iPS-MPs. We observed a significant increase only at a percentage of 25% mutant macrophages (Figure 4C). Thus, we capitulated, at least in part, the patient's mosaic condition in vitro.

Next, we tried to elucidate whether the interaction is mediated by some humoral factor(s), but supernatant transfer did not facilitate the IL-1β secretion (Figure 4D). As a candidate that may mediate this interaction, we selected ATP because necrotic cells trigger NLRP3-inflammasome activation in part through ATP release.[24] We therefore investigated whether the necrosis-induced ATP secretion activates the wild-type iPS-MPs using ATP receptor antagonists, oxidized ATP (oATP) and PPADS. Although both antagonists markedly inhibited the IL-1β secretion after LPS plus ATP stimulation (supplemental Figure 4B), neither of them abrogated the additional IL-1β secretion in the mixed culture (Figure 4E; compare column 2 with column 3, and column 4 with column 5). The IL-1β secretion from mutant iPS-MPs may have decreased because of off-target effects of oATP.[25] Overall, although it remains to be elucidated how this effect is mediated, these results suggest that the interaction between mutant and wild-type macrophages may enhance IL-1β secretion in mosaic patients.

Validation for future applications for drug screening

An NLRP3-targeted therapeutic approach would be attractive because (1) the progressive arthropathy despite anti–IL-1 therapy indicates that the presence of additional proteins processed by the

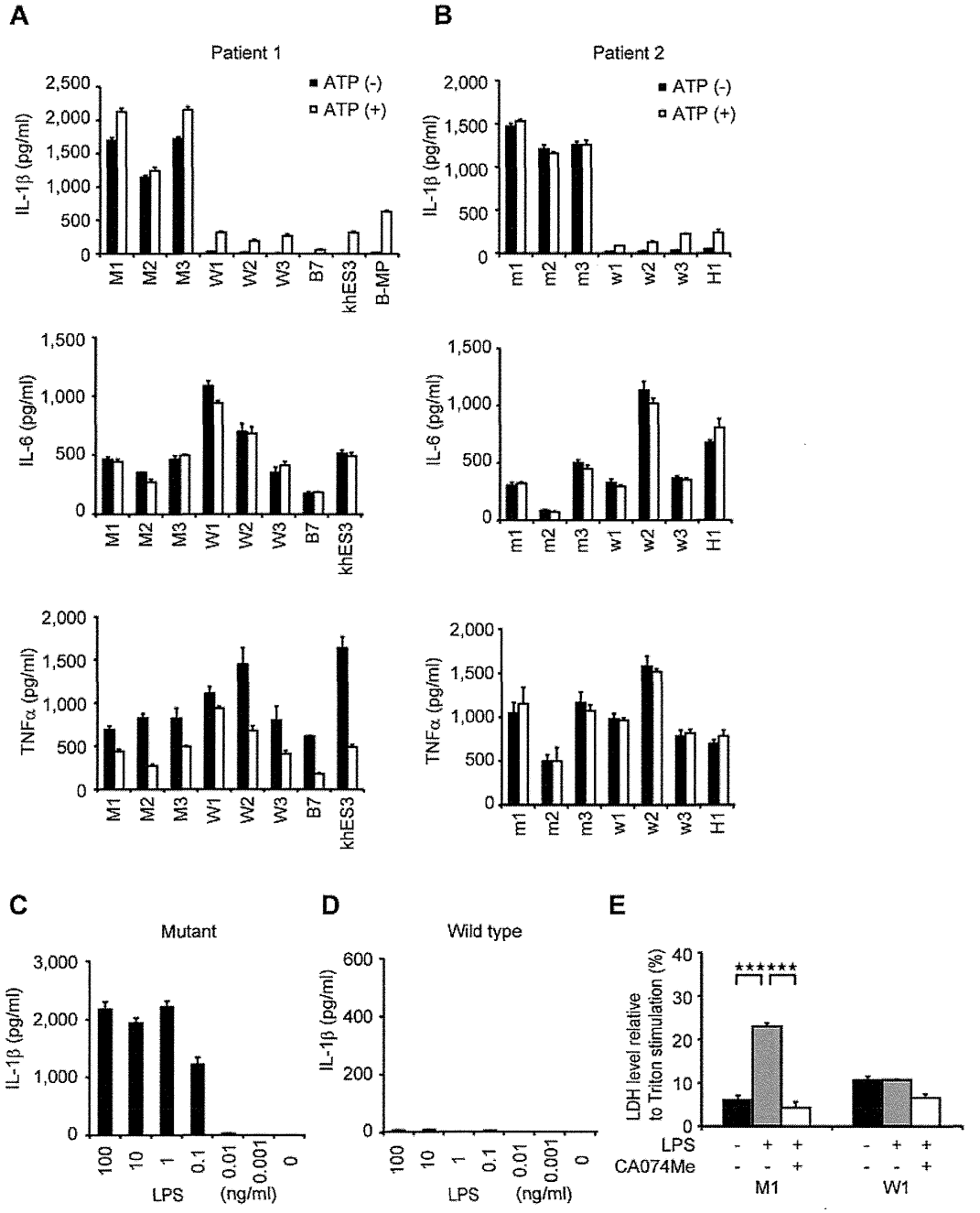

Figure 3. Elucidation of the pathogenesis of somatic mosaic CINCA syndrome. (A) Cytokine secretion from iPS-MPs derived from patient 1. After stimulating iPS-MPs by LPS with or without ATP, we determined the IL-1β (top panel), IL-6 (middle panel), or TNFα (bottom panel) level of the supernatant. n = 3. (B) Cytokine secretion from iPS-MPs derived from patient 2, determined as in panel A. (C) IL-1β secretion from mutant iPS-MPs in the presence of 10-fold dilutions of LPS from 100 ng/mL. n = 3. (D) IL-1β secretion from wild-type iPS-MPs, determined as in panel C. (E) LDH secretion from iPS-MPs stimulated with LPS in the presence or absence of the cathepsin B inhibitor, CA074Me. n = 3. Data are mean ± SEM. ***$P < .001$ (Student t test).

inflammasome is also involved in the pathogenesis of CINCA syndrome; (2) specific inhibition of the NLRP3-inflammasome can avoid unfavorable suppression of other IL-1β–processing pathways in response to various triggers; and (3) these drugs may be also effective for various other NLRP3-related chronic inflammatory conditions, such as Alzheimer disease, diabetes, severe gout, and atherosclerosis.[26-30] Because drug screening using NLRP3 autoactivated cells has not been described previously, we examined whether the iPS-MPs from CINCA patients can serve as a prototype for seeking drug candidates that directly modulate NLRP3-inflammasome activation.

When wild-type iPS-MPs were stimulated with LPS and ATP in the presence of various inhibitors, inhibitors known to modulate molecules upstream of the NLRP3-inflammasome (a protein synthesis inhibitor, cycloheximide, and an NF-κB inhibitor, MG132), downstream of the inflammasome (a caspase-1 inhibitor, Ac-YVAD-CHO), and both upstream of and the inflammasome itself[31] (Bay11-7082) successfully inhibited IL-1β secretion (Figure 5A). Although the precise mechanism is unknown, a cathepsin B inhibitor, CA074Me, also efficiently inhibited IL-1β secretion. As expected, upstream inhibitors inhibited the secretion of other cytokines, such as IL-6 and IL-8, but a downstream inhibitor,

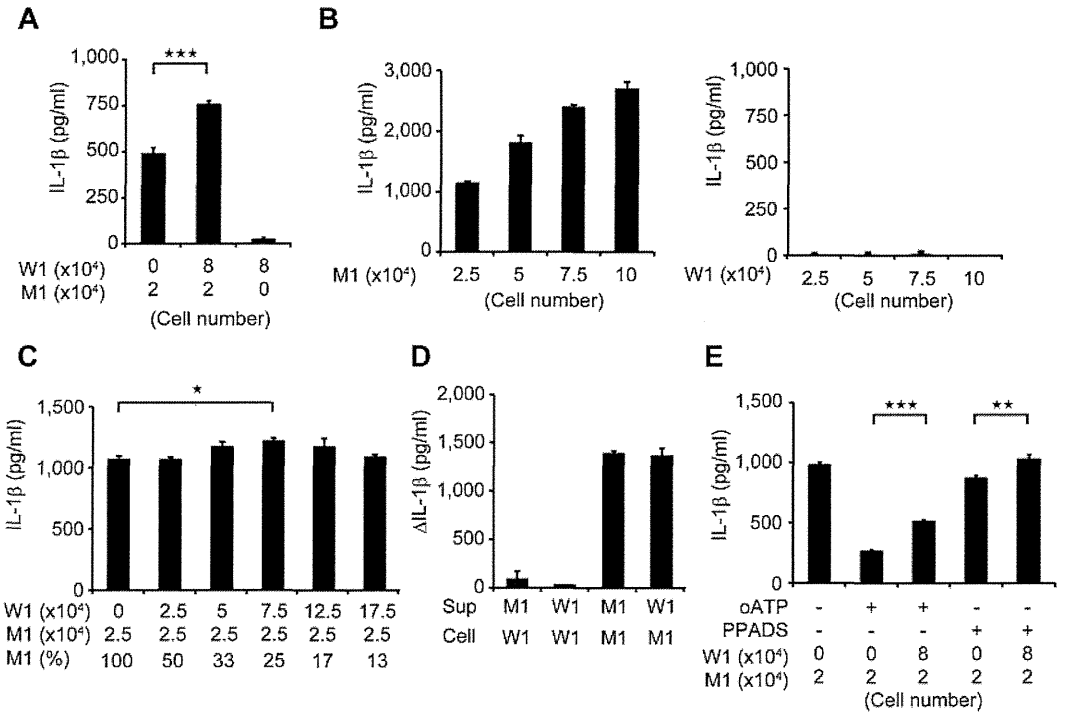

Figure 4. Remodeling mosaicism by coculturing mutant and wild-type iPS-MPs. (A) IL-1β secretion from cocultured iPS-MPs. We used 2 × 10^4 mutant iPS-MPs (M1) and 8 × 10^4 wild-type iPS-MPs (W1) as indicated. n = 6. (B) IL-1β secretion from various numbers of mutant (left panel) or wild-type (right panel) iPS-MPs. The iPS-MPs were seeded at the indicated numbers. n = 3. (C) IL-1β secretion from iPS-MPs that were cocultured at various ratios. The wild-type or mutant iPS-MPs were seeded at the numbers indicated in the first and second rows, respectively. The percentage of mutants is indicated in the third row; n = 3. (D) Increase of IL-1β levels during stimulation by the supernatant. The supernatant was harvested from the wells of the indicated iPS-MPs (Sup) and transferred to the wells of other iPS-MPs (Cell); n = 3. (E) IL-1β secretion from cocultured iPS-MPs in the presence of the ATP receptor antagonist, oATP (300μM) or PPADS (300μM). We used 2 × 10^4 mutant iPS-MPs (M1) and 8 × 10^4 wild-type iPS-MPs (W1) as indicated. n = 6. Data are mean ± SEM. ***$P < .001$ (Student *t* test). **$P < .01$ (Student *t* test). *$P < .05$ (Student *t* test).

Ac-YVAD-CHO, specifically affected IL-1β secretion (Figure 5A). Although CA074Me and Ac-YVAD-CHO inhibited IL-1β secretion regardless of the second signals that were present, PPADS, an inhibitor of extracellular ATP signaling, failed to inhibit IL-1β secretion by following exposure to other second signals, such as monosodium urate and silica crystals (Figure 5B), proving that wild-type iPS-MPs can be activated in a second signal-dependent manner. Therefore, the results of the wild-type iPS-MP-based compound screening depended on the choice of second signals, and such a screening makes it possible to extract candidate compounds that modulate specific second signaling pathways.

Next, we examined the response of mutant iPS-MPs to the inhibitors. In the absence of inhibitors, mutant iPS-MPs secreted a higher level of IL-1β, but treatment with inhibitors dose-dependently decreased IL-1β secretion to the comparable level produced by WT iPS-MPs (Figure 5C). We thus demonstrated the efficacy of these chemical compounds, even for excessive IL-1β production by constitutively hyperactivated inflammasomes. As expected, the mutant iPS-MPs did not respond to PPADS, confirming their autoactivation in a second signal-independent manner (Figure 5D). Therefore, because they can be activated independently from the type of second signals, mutant iPS-MP–based screening would enable the exclusion of compounds that inhibit IL-1β secretion depending on a specific type of second signal transduction. Overall, through using the IL-1β inhibition as the initial criteria and weeding out upstream inhibitors by measuring the levels of other cytokines, we can use *NLRP3*-mutant iPS-MPs to screen for drugs for CINCA syndrome and possibly for other NLRP3-related chronic inflammatory conditions.

Discussion

Since the first identification of a CINCA syndrome patient carrying *NLRP3* mutation as somatic mosaicism,[20] it has been controversial whether the small fraction of *NLRP3*-mutated cells actually causes the strong autoinflammation. It remained unanswered because of the difficulty to separately obtain live mutant and nonmutant blood cells. In this study, we reprogrammed fibroblasts from mosaic patients and obtained macrophages with different genotypes. By showing that only *NLRP3*-mutant iPS-MPs exhibit the distinct proinflammatory phenotype, we demonstrated that the *NLRP3*-mutant macrophages are mainly responsible for the pathogenesis of mosaic CINCA syndrome.

In this study, we established both *NLRP3*-mutant and nonmutant iPSC clones from the same person. One of the potential limitations of studies with patient-derived iPSCs is the difficulty in obtaining isogenic control counterparts, which do not carry the responsible mutations. One possible strategy to solve this problem is to correct the affected gene locus of patient-derived iPSC clones using novel techniques that facilitate homologous recombination.[32,33] As another solution, both affected and control iPSC clones can be obtained from patients of some X-linked hereditary diseases because each iPSC clone originated from somatic cells carrying either a mutated or nonmutated allele as an active X chromosome.[34-36] In the present study, we have retrieved both mutant and wild-type iPSC clones from patients with somatic autosomal mutations. These clones theoretically have the same genetic backgrounds, except for the *NLRP3* gene, and should serve as an ideal pair of mutant and control clones for disease research.

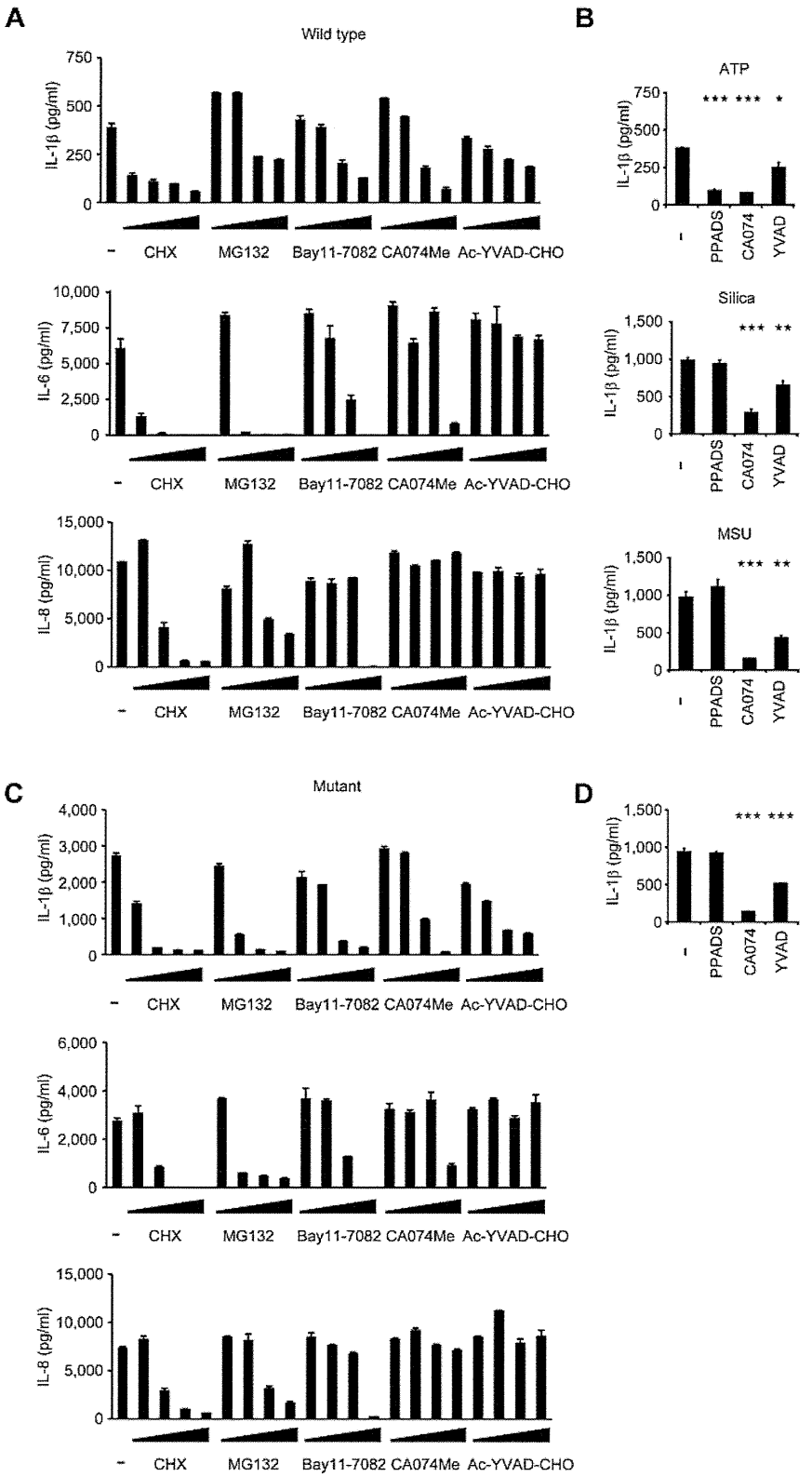

Figure 5. Validation of the cells for future applications for drug screening. (A) Inhibition of IL-1β (top panel), IL-6 (middle panel), or IL-8 (bottom panel) secretion from wild-type iPS-MPs by various inhibitors. The iPS-MPs were cultured for 2 hours in the presence of 100μM cycloheximide (CHX), 100μM MG132, 10μM Bay11-7082, 25μM CA074Me, 50μM Ac-YVAD-CHO, as well as 10-fold dilutions of each inhibitor, except CA074Me (which was diluted 5-fold), followed by LPS treatment plus ATP stimulation. n = 3. (B) The differential inhibition of IL-1β secretion from wild-type iPS-MPs by various inhibitors. In the presence of inhibitors, such as PPADS (300μM), CA074Me (25μM), or Ac-YVAD-CHO (50μM), LPS-primed wild-type iPS-MPs were stimulated with second signal triggers, such as ATP for 1 hour (top panel), silica crystals for 1 hour (middle panel), or monosodium urate crystals for 3 hours (bottom panel). n = 3. (C) Inhibition of IL-1β (top panel), IL-6 (middle panel), or IL-8 (bottom panel) secretion from mutant iPS-MPs by various inhibitors was evaluated as in panel A; n = 3. (D) Inhibition of IL-1β secretion from mutant iPS-MPs by various inhibitors. In the presence of inhibitors, such as PPADS (300μM), CA074Me (25μM), or Ac-YVAD-CHO (50μM), mutant iPS-MPs were stimulated with LPS for 4 hours. n = 3. Data are mean ± SEM. ***$P < .001$ (Student t test). **$P < .01$ (Student t test). *$P < .05$ (Student t test).

In addition to obtaining isogenic controls, iPSCs from patients with somatic autosomal mutations enable dissection and modeling of somatic mosaicism. Despite the fact that each person contains various minor somatic mutations,[37] the effects of mosaicism can often be overlooked because of the difficulty in assessing the possible biologic effects caused by the small cell populations carrying the genetic alterations. Here we dissected somatic mosaicism by obtaining the component cells with heterogeneous genetic identity separately and established an in vitro model to evaluate the interaction between these cells, although precise mechanism of interaction remains to be elucidated. As an approach to determining the disease-causing potential of a specific somatic mutation found in a person, iPSC technology provides advantages compared with ordinary methods, such as the use of transgenic cell lines. First,

iPSCs can be differentiated into the affected cell types or tissues, allowing direct functional assays to be performed that are associated with the pathology. Second, because the disease-causing potential of some mutations is dependent on the genetic backgrounds of the patients,[38] it may be better to obtain both mutant and wild-type clones from a single mosaic patient to more accurately assess the impact of the mutation(s).

Considering that a mutation of *NLRP3* in 10% of the cells is sufficient to cause a distinct disease phenotype, somatic mutations of various genes at an even rarer frequency may also affect the biologic characteristics of a person. Because the presence of the *NLRP3* mutation did not affect the efficacy of reprogramming to the iPSCs, we may be able to obtain both mutant and wild-type iPSC clones from CINCA syndrome patients who carry *NLRP3* mutant cells at a lower percentage. In some diseases, such as Fanconi anemia, however, mutant cells may be resistant to reprogramming.[39,40] Even though there are some possible limitations, establishing both mutant and wild-type iPSC clones is a promising approach to dissect the extent and role of somatic mosaicism.

We demonstrated that several inhibitors that are considered to be effective against CINCA syndrome actually attenuated the disease-relevant phenotype of iPSC-derived macrophages. Before a successful drug screening using iPSC-derived somatic cells can be developed, several limitations need to be overcome, such as the heterogeneity of differentiation and difficulties associated with purification.[18] In this report, we used an efficient and robust differentiation protocol and obtained plenty of macrophages free from the clonal variations.

In conclusion, we elucidated the pathologic roles of both mutant and wild-type cells in mosaic CINCA syndrome patients. After obtaining iPSC-derived macrophages in large quantity and with high purity, we showed they are applicable for drug screening. The iPSC-based approach may help to illuminate the pathogenesis of various diseases that are caused by somatic mosaicism, and facilitate drug discovery for the treatment of NLRP3-related inflammatory diseases.

Acknowledgments

The authors thank the CINCA syndrome patients who participated in this study; Y. Sasaki, Y. Jindai, A. Okada, M. Narita, A. Nagahashi, T. Ohkame, S. Nishimoto, Y. Inoue, and S. Arai for technical assistance; I. Kato for help with animal experiments; M. Nakagawa, K. Okita, Y. Yoshida, T. Aoi, and M. Yanagimachi for scientific comments; and R. Kato, E. Nishikawa, S. Takeshima, Y. Otsu, H. Hasaba, H. Watanabe, T. Ishii, H. Kurokawa, N. Takasu, and Y. Takao for administrative assistance.

This work was supported by the Ministry of Health, Labor and Welfare (N.M. and T.N.), the Ministry of Education, Culture, Sports, Science and Technology (MEXT; N.M. and T.N.), the Leading Project of MEXT (S.Y. and T.N.), the Promotion of Fundamental Studies in Health Sciences of National Institute of Biomedical Innovation (S.Y.), the Funding Program for World-Leading Innovative Research and Development on Science and Technology (FIRST Program) of Japan Society for the Promotion of Science (JSPS; T.N., and S.Y.), JSPS and MEXT (Grants-in-Aid for Scientific Research; S.Y.), JSPS (T.N., T.T., and M.K.S.), the Takeda Science Foundation, SENSHIN Medical Research Foundation, and Suzuken Memorial Foundation to (M.K.S.).

Authorship

Contribution: T.T. planned the project, established iPSCs, performed experimental work, analyzed data, and prepared the manuscript; K.T. planned the project, established iPSCs, and analyzed data; M.Y., S.T., and S.N. performed experimental work; K.O., A.N., and T.H. analyzed data; R.N. and N.K. planned the project; H.H. and M.M. performed *L monocytogenes* infection; N.M. and J.E.H. performed electron microscopy; T.Y. identified retroviral integration sites; A.W. performed bisulfite sequencing; A.S.-O. and S.O. analyzed CNV; I.A. established iPSCs; S.Y. and T.N. planned the project and analyzed data; M.K.S. planned the project, analyzed data, and prepared the manuscript; and all authors read and approved the manuscript.

Conflict-of-interest disclosure: S.Y. is a member without salary of the scientific advisory boards of iPierian, iPS Academia Japan, and Megakaryon Corporation. The remaining authors declare no competing financial interests.

Correspondence: Megumu K. Saito, Center for iPS Cell Research and Application, Kyoto University, Kyoto 606-8507, Japan; e-mail: msaito@cira.kyoto-u.ac.jp.

References

1. Prieur AM, Griscelli C, Lampert F, et al. A chronic, infantile, neurological, cutaneous and articular (CINCA) syndrome: a specific entity analysed in 30 patients. *Scand J Rheumatol Suppl.* 1987;66: 57-68.
2. Aksentijevich I, Nowak M, Mallah M, et al. De novo CIAS1 mutations, cytokine activation, and evidence for genetic heterogeneity in patients with neonatal-onset multisystem inflammatory disease (NOMID): a new member of the expanding family of pyrin-associated autoinflammatory diseases. *Arthritis Rheum.* 2002;46(12):3340-3348.
3. Feldmann J, Prieur AM, Quartier P, et al. Chronic infantile neurological cutaneous and articular syndrome is caused by mutations in CIAS1, a gene highly expressed in polymorphonuclear cells and chondrocytes. *Am J Hum Genet.* 2002;71(1):198-203.
4. Bauernfeind FG, Horvath G, Stutz A, et al. Cutting edge: NF-kappaB activating pattern recognition and cytokine receptors license NLRP3 inflammasome activation by regulating NLRP3 expression. *J Immunol.* 2009;183(2):787-791.
5. Mariathasan S, Weiss DS, Newton K, et al. Cryopyrin activates the inflammasome in response to toxins and ATP. *Nature.* 2006; 440(7081):228-232.
6. Gattorno M, Tassi S, Carta S, et al. Pattern of interleukin-1beta secretion in response to lipopolysaccharide and ATP before and after interleukin-1 blockade in patients with CIAS1 mutations. *Arthritis Rheum.* 2007;56(9):3138-3148.
7. Goldbach-Mansky R, Dailey NJ, Canna SW, et al. Neonatal-onset multisystem inflammatory disease responsive to interleukin-1beta inhibition. *N Engl J Med.* 2006;355(6):581-592.
8. Neven B, Marvillet I, Terrada C, et al. Long-term efficacy of the interleukin-1 receptor antagonist anakinra in ten patients with neonatal-onset multisystem inflammatory disease/chronic infantile neurologic, cutaneous, articular syndrome. *Arthritis Rheum.* 2010;62(1):258-267.
9. Saito M, Nishikomori R, Kambe N, et al. Disease-associated CIAS1 mutations induce monocyte death, revealing low-level mosaicism in mutation-negative cryopyrin-associated periodic syndrome patients. *Blood.* 2008;111(4):2132-2141.
10. Tanaka N, Izawa K, Saito MK, et al. High incidence of NLRP3 somatic mosaicism in patients with chronic infantile neurologic, cutaneous, articular syndrome: results of an International Multicenter Collaborative Study. *Arthritis Rheum.* 2011;63(11):3625-3632.
11. Masters SL, Simon A, Aksentijevich I, Kastner DL. Horror autoinflammaticus: the molecular pathophysiology of autoinflammatory disease. *Annu Rev Immunol.* 2009;27:621-668.
12. Youssoufian H, Pyeritz RE. Mechanisms and consequences of somatic mosaicism in humans. *Nat Rev Genet.* 2002;3(10):748-758.
13. Erickson RP. Somatic gene mutation and human disease other than cancer: an update. *Mutat Res.* 2010;705(2):96-106.
14. Ariga T, Kondoh T, Yamaguchi K, et al. Spontaneous in vivo reversion of an inherited mutation in the Wiskott-Aldrich syndrome. *J Immunol.* 2001; 166(8):5245-5249.

15. Nishikomori R, Akutagawa H, Maruyama K, et al. X-linked ectodermal dysplasia and immunodeficiency caused by reversion mosaicism of NEMO reveals a critical role for NEMO in human T-cell development and/or survival. *Blood.* 2004; 103(12):4565-4572.
16. Lutskiy MI, Beardsley DS, Rosen FS, Remold-O'Donnell E. Mosaicism of NK cells in a patient with Wiskott-Aldrich syndrome. *Blood.* 2005;106(8):2815-2817.
17. Takahashi K, Tanabe K, Ohnuki M, et al. Induction of pluripotent stem cells from adult human fibroblasts by defined factors. *Cell.* 2007;131(5): 861-872.
18. Grskovic M, Javaherian A, Strulovici B, Daley GQ. Induced pluripotent stem cells: opportunities for disease modelling and drug discovery. *Nat Rev Drug Discov.* 2011;10(12):915-929.
19. Hanna J, Markoulaki S, Schorderet P, et al. Direct reprogramming of terminally differentiated mature B lymphocytes to pluripotency. *Cell.* 2008;133(2): 250-264.
20. Saito M, Fujisawa A, Nishikomori R, et al. Somatic mosaicism of CIAS1 in a patient with chronic infantile neurologic, cutaneous, articular syndrome. *Arthritis Rheum.* 2005;52(11):3579-3585.
21. Nakano T, Kodama H, Honjo T. Generation of lymphohematopoietic cells from embryonic stem cells in culture. *Science.* 1994;265(5175):1098-1101.
22. Fujisawa A, Kambe N, Saito M, et al. Disease-associated mutations in CIAS1 induce cathepsin B-dependent rapid cell death of human THP-1 monocytic cells. *Blood.* 2007;109(7):2903-2911.
23. Willingham SB, Bergstralh DT, O'Connor W, et al. Microbial pathogen-induced necrotic cell death mediated by the inflammasome components CIAS1/cryopyrin/NLRP3 and ASC. *Cell Host Microbe.* 2007;2(3):147-159.
24. Iyer SS, Pulskens WP, Sadler JJ, et al. Necrotic cells trigger a sterile inflammatory response through the Nlrp3 inflammasome. *Proc Natl Acad Sci U S A.* 2009;106(48):20388-20393.
25. Beigi RD, Kertesy SB, Aquilina G, Dubyak GR. Oxidized ATP (oATP) attenuates proinflammatory signaling via P2 receptor-independent mechanisms. *Br J Pharmacol.* 2003;140(3):507-519.
26. Martinon F, Petrilli V, Mayor A, Tardivel A, Tschopp J. Gout-associated uric acid crystals activate the NALP3 inflammasome. *Nature.* 2006; 440(7081):237-241.
27. Halle A, Hornung V, Petzold GC, et al. The NALP3 inflammasome is involved in the innate immune response to amyloid-beta. *Nat Immunol.* 2008;9(8):857-865.
28. Duewell P, Kono H, Rayner KJ, et al. NLRP3 inflammasomes are required for atherogenesis and activated by cholesterol crystals. *Nature.* 2010; 464(7293):1357-1361.
29. Masters SL, Dunne A, Subramanian SL, et al. Activation of the NLRP3 inflammasome by islet amyloid polypeptide provides a mechanism for enhanced IL-1beta in type 2 diabetes. *Nat Immunol.* 2010;11(10):897-904.
30. Vandanmagsar B, Youm YH, Ravussin A, et al. The NLRP3 inflammasome instigates obesity-induced inflammation and insulin resistance. *Nat Med.* 2011;17(2):179-188.
31. Juliana C, Fernandes-Alnemri T, Wu J, et al. Anti-inflammatory compounds parthenolide and Bay 11-7082 are direct inhibitors of the inflammasome. *J Biol Chem.* 2010;285(13):9792-9802.
32. Aizawa E, Hirabayashi Y, Iwanaga Y, et al. Efficient and accurate homologous recombination in hESCs and hiPSCs using helper-dependent adenoviral vectors. *Mol Ther.* 2012;20(2):424-431.
33. Soldner F, Laganiere J, Cheng AW, et al. Generation of isogenic pluripotent stem cells differing exclusively at two early onset Parkinson point mutations. *Cell.* 2011;146(2):318-331.
34. Cheung AY, Horvath LM, Grafodatskaya D, et al. Isolation of MECP2-null Rett syndrome patient hiPS cells and isogenic controls through X-chromosome inactivation. *Hum Mol Genet.* 2011;20(11):2103-2115.
35. Kim KY, Hysolli E, Park IH. Neuronal maturation defect in induced pluripotent stem cells from patients with Rett syndrome. *Proc Natl Acad Sci U S A.* 2011;108(34):14169-14174.
36. Pomp O, Dreesen O, Leong DF, et al. Unexpected X chromosome skewing during culture and reprogramming of human somatic cells can be alleviated by exogenous telomerase. *Cell Stem Cell.* 2011;9(2):156-165.
37. Gore A, Li Z, Fung HL, et al. Somatic coding mutations in human induced pluripotent stem cells. *Nature.* 2011;471(7336):63-67.
38. Crotti L, Lundquist AL, Insolia R, et al. KCNH2-K897T is a genetic modifier of latent congenital long-QT syndrome. *Circulation.* 2005;112(9): 1251-1258.
39. Raya A, Rodriguez-Piza I, Guenechea G, et al. Disease-corrected haematopoietic progenitors from Fanconi anemia induced pluripotent stem cells. *Nature.* 2009;460(7251):53-59.
40. Müller LU, Milsom MD, Harris CE, et al. Overcoming reprogramming resistance of Fanconi anemia cells. *Blood.* 2012;119(23):5449-5457.

EUROPEAN JOURNAL OF Haematology

European Journal of Haematology 89 (350–355)

CASE REPORT

CD20 gene deletion causes a CD20-negative relapse in diffuse large B-cell lymphoma

Tsuyoshi Nakamaki[1], Kunihiko Fukuchi[2], Hidetoshi Nakashima[1], Hirotsugu Ariizumi[1], Takashi Maeda[1], Bungo Saito[1], Kouji Yanagisawa[1], Shigeru Tomoyasu[1], Mayumi Homma[3], Eisuke Shiozawa[3], Toshiko Yamochi-Onizuka[3], Hidekazu Ota[3]

[1]Division of Hematology, Department of Medicine, Showa University School of Medicine; [2]Department of Clinical Pathology, Showa University School of Medicine; [3]Department of Pathology, Showa University School of Medicine, Tokyo, Japan

Abstract

In diffuse large B-cell lymphoma (DLBCL), a CD20-negative relapse is clinically significant because it is associated with chemo-refractory phenotypes and loss of a therapeutic target. The alteration of the CD20 gene is reported as infrequent in CD20-negative relapse in B-cell lymphoma. We established a DLBCL cell line with loss of CD20 expression (SD07) from a patient at CD20-negative relapse. She was initially diagnosed with CD20-positive DLBCL and received repeated immuno-chemotherapy that included rituximab. SD07, which has an immunoglobulin κ rearrangement identical to that of lymphoma cells at CD20-negative relapse, showed homozygous deletion of the CD20 gene with loss of the copy number of 11q12. SD07 is the first case in which it is proven that the loss of CD20 expression in relapsed DLBCL is the result of deletion of the CD20 gene. Deletion of the CD20 gene is a molecular mechanism of CD20-negative relapse in a subset of DLBCL.

Key words diffuse large B-cell lymphoma; CD20; deletion

Correspondence Tsuyoshi Nakamaki, 1-5-8 Hatanodai, Shinagawa-Ku, Tokyo 142-8666, Japan. Tel: +81-3-3784-8338; Fax: +81-3-3784-8250; e-mail: nakamaki@med.showa-u.ac.jp

Accepted for publication 11 July 2012

doi:10.1111/j.1600-0609.2012.01838.x

Case report

Studies show that the expression of CD20, an activated-glycosylated phosphoprotein that is widely expressed in mature B-cell neoplasm, is decreased or lost in instances of CD20-negative relapse that occur after receiving immuno-chemotherapy that includes rituximab, a chimeric anti-CD20 antibody (1). CD20-negative relapse is now well-recognized in various types of B-cell lymphomas (2). In diffuse large B-cell lymphoma (DLBCL), CD20-negative relapse was found through immunohistochemical analysis to be present in about 15% of re-biopsied tissues after relapse (3). Importantly, in DLBCL, a CD20-negative relapse is often associated with chemo-refractory phenotypes and a poor prognosis for the patient, in addition to the loss of a therapeutic target (1, 3).

It is necessary to clarify the molecular mechanism(s) underlying the development of CD20-negative relapse to overcome rituximab-resistant relapse. The loss of expression of the CD20 protein in B-cell lymphoma cells is the result of a complex mechanism (1, 4). Genomic alteration of the *CD20* gene, which is involved in the loss of expression, is infrequent in the previous report (3, 5), although deletional mutation(s) of the *CD20* gene was associated with the decreased expression of CD20 in DLBCL progression (6). In this study, we report the homozygous deletion of the *CD20* gene in a CD20-negative relapse in a case of DLBCL.

A 68-yr-old female was admitted to our hospital reporting fever and bilateral leg edema. A computed tomography (CT) scan showed significant para-aortic lymph node swelling and left hydronephrosis. A CT-guided needle biopsy was performed, and the histopathological diagnosis was DLBCL (Fig. 1A[a, b]). Immunohistochemically, more than 80% of the lymphoma cells were positive for CD20 (L26) (Fig. 1A[c, d]). After 2 yrs and 3 months of repeated anti-lymphoma therapy, including rituximab, the patient developed massive right pleural effusion infiltrated with lymphoma cells (Fig. 1B[a]). These cells were positive for CD19, but not for CD20, as eval-

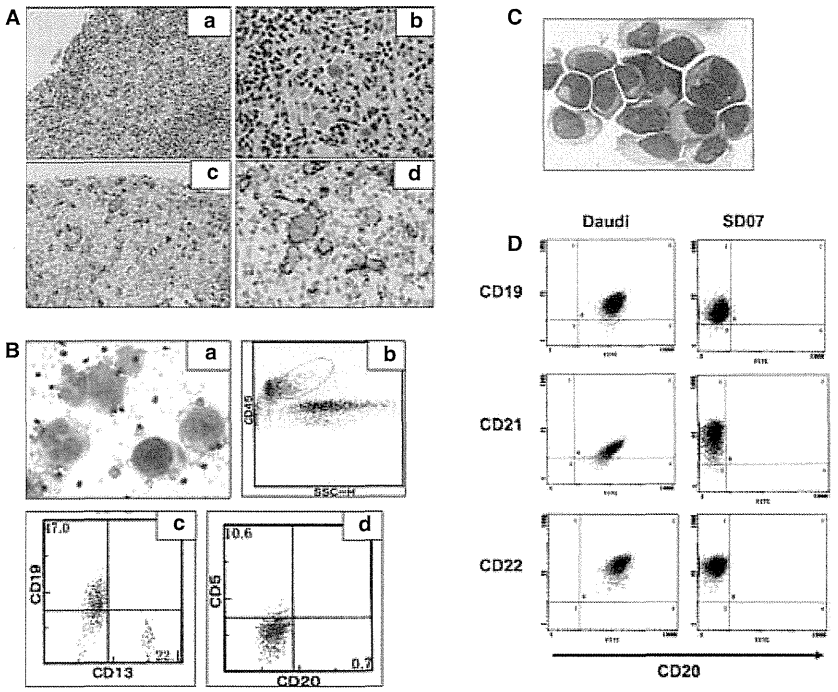

Figure 1 Establishment of CD20-negative DLBCL cell line, SD07. (A) Histopathology of needle biopsy specimens of an abdominal lymph node in a 68-yr–old patient at diagnosis (a–d). (a) Hematoxylin eosin (HE) stain,(b)HE stain (higher magnification), (c) anti-CD20 (L26, Dako Cytomation, Glostrup, Denmark) and (d) anti-CD20 (higher magnification). (B) Cell morphology and flow cytometric (FCM) analyses of lymphoma cells that appeared in pleural effusion at relapse(a–d). (a) Giemsa stain of lymphoma cells in pleural effusion. (b) Lymphoma cell gating based on SSC and expression of CD45. (c) Histogram of lymphoma cells stained by CD19-PE (Beckman Coulter Inc. [BC], Brea, CA, USA) and CD13-FITC (Dako). (d) Histogram of lymphoma cells stained by CD5-PE (BC) and CD20-FITC (Dako). (C) May-Giemsa stain of SD07 cells. (D) FCM analyses of cell surface B-cell antigens of a Burkitt lymphoma cell line, Daudi and SD07. Both cells are stained by CD19-PE (BD Transduction Laboratories [BD], San Jose, CA, USA) and CD20-FITC (BD); CD21-PE (BioLegend, San Diego, CA, USA) and CD20-FITC (BD), or CD22-PE (BC) and CD20-FITC (BD). Two-color analyses of these expressions were performed with a flow cytometer (Coulter EPICS XL).

uated by flow cytometry (FCM) (Fig. 1B[b–d]). The patient died 2 months after the CD20-negative relapse. An autopsy showed that CD20-negative lymphoma cells had infiltrated multiple lymph nodes as well as extra-nodal organs.

SD07, a DLBCL cell line, was established from lymphoma cells obtained from the pleural effusion of this patient. The lymphoma cells were obtained with informed consent, and the protocols approved by our institution's ethics committee. The SD07 was cultured in an RPMI1640 medium supplemented with 10% fetal calf serum (FCS), which had been maintained in my laboratory for more than 4 yrs. Morphologically, SD07 cells are large lymphoid cells (Fig. 1C). As evaluated by FCM, SD07 cells selectively lack CD20 protein expression, yet express other B-cell antigens, such as CD19, CD21, and CD22, at the same levels as those of Daudi, Burkitt lymphoma cells (Fig. 1D).

In severe combined immunodeficiency (SCID) mice, subcutaneously transplanted SD07 cells (10^7 cells) developed subcutaneous tumors 2 months after inoculation (Fig. 2A). Animal experiments were performed according to a protocol approved by the Institutional Animal Care and Use committee of Showa University. Histopathologically, the tumor consisted of large lymphoid cells (Fig. 2B), which were positive for B-cell antigens such as CD79a, Pax5, and Oct2, but not CD20 (L26) (Fig. 2C–F). *In situ* hybridization showed lymphoma cells were negative for Epstein–Barr virus (EBV)-encoded RNA (EBER), which suggests that the activation of EBV was not involved in SD07 (Fig. 2G).

By polymerase chain reaction (PCR) and sequencing analysis, the SD07 cells and SCID tumor produced clonal 149bp *IGK* gene rearrangement (V1-8-J4) bands identical to those in the lymphoma cells that infiltrated the pleural effusion of this patient (Figure S1). This suggests that SD07 is clonally identical to the lymphoma cells that appeared with the CD20-negative relapse of this patient.

A karyotype analysis of the SD07 showed near-tetraploid chromosomes as follows: 83~90, XX, −X, −X or −Y, −Y, −2, add(3)(p11), add(3)(q11), add(3)(q12), −4, −4, −6, −7, −7, +8, add(8)(q22)×2, −9, −9, −11, −11, add(11)(q23)×2, −12, −14, −14, −15, −15, −16, −16, −17, add(18)(q21)×2, −20, −22, −22, −22, +mar1×2, +mar2, +mar3, and +mar4 (Figure S2).

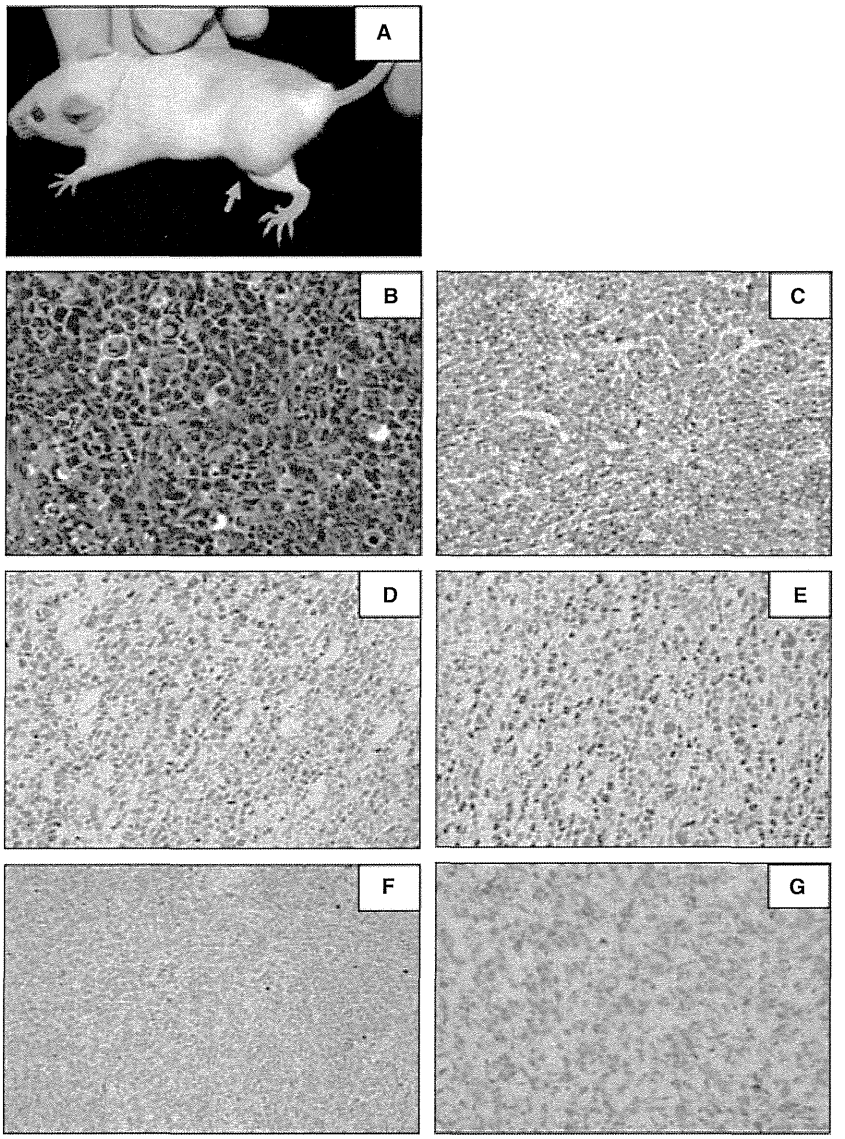

Figure 2 Subcutaneous tumor of SD07 transplanted in an SCID mouse (A–G). (A) A tumor (orange arrow) in the left hip of an SCID mouse appeared 2 months after subcutaneous transplantation of 10^7 cells of SD07 cells. Histopathology of the subcutaneous tumor, (B) HE stain, immunostaining with (C) anti-CD79a (Dako), (D) anti-Pax5 (BD), (E) anti-Oct-2 (Santa Cruz Biotechnology Inc.[SC], Santa Cruz, CA, USA), (F) anti-CD20 (Dako), or (G) Epstein–Barr virus (EBV)-encoded small RNA (EBER)(Dako) analyzed as *in situ* hybridization

To analyze the details of genomic alteration involved in the loss of expression of CD20 in SD07, we performed array comparative genomic hybridization (CGH). Genomic DNA from this patient extracted from bone marrow cells without infiltration of lymphoma cells was used as a reference. It revealed a 0.7 megabase (Mb) region with a copy number loss of -1.0 of $\log_2$ ratios on chromosome 11q12 in SD07 (Fig. 3A). Within this region, a 30-kilobase (kb) segment showed further loss (less than -2.0) and contained two genes, *MS4A1(CD20)* and *MS4A5* (Fig. 3A).

A Southern blot analysis, using the *CD20* gene Exon 1 as a probe, showed homozygous deletion of the *CD20* gene in SD07 (Fig. 3B). As expected, an RT-PCR analysis revealed a lack of mRNA expression of CD20 in SD07 (Figure S3A). An epigenetic modification with both 5-aza-2′-deoxycytidine and trichosatine A in a culture failed to induce RNA expression of CD20 in SD07 (Figure S3A). Through Western blotting, CD20 protein expression was not detected in SD07 (Figure S3B). Incubation with rituximab in a culture failed to suppress the cell growth of SD07 up to 20 μg/mL (Figure S4). This suggests that deletion of the *CD20* gene with genomic copy number loss in 11q12 produced the loss of CD20 expression and resulted in resistance to rituximab in SD07. On the basis of the literature to date, SD07 is the first case in which it is proven that the loss of CD20 expression in relapsed DLBCL is the result of deletion of the *CD20* gene.